ISSN 1075-7015, Geology of Ore Deposits, 2015, Vol. 57, No. 4, pp. 292–312. © Pleiades Publishing, Ltd., 2015.
Original Russian Text © V.A. Petrov, Yu.L. Rebetsky, V.V. Poluektov, A.A. Burmistrov, 2015, published in Geologiya Rudnykh Mestorozhdenii, 2015, Vol. 57, No. 4, pp. 327–350.

Tectonophysics of Hydrothermal Ore Formation: an Example of the Antei Mo–U Deposit, Transbaikalia

V. A. Petrov[a], Yu. L. Rebetsky[b], V. V. Poluektov[a], and A. A. Burmistrov[c]

[a] *Institute of Geology of Ore Deposits, Petrography, Mineralogy and Geochemistry, Russian Academy of Sciences, Staromonetny per. 35, Moscow, 119017 Russia*

[b] *Schmidt Institute of Physics of the Earth, Russian Academy of Sciences, ul. B. Gruzinskaya 10, Moscow, 123995 Russia*

[c] *Moscow State University, Leninskie Gory 1, Moscow, 119991 Russia*

Received March 10, 2015

Abstract—The Antei deposit of the southeastern Transbaikalian region is one of the largest uranium mines in Russia. It is hosted by the Late Paleozoic granitic basement of the Streltsovskaya caldera and was formed as a result of Late Mesozoic tectonothermal activity. Vein and stockwork–disseminated molybdenum–uranium mineralization at this deposit is controlled by zones of intense hydrothermal alteration, cataclasis, brecciation, and intense fracturing along steeply dipping faults, which acted as conduits for mineralizing fluids and hosts to the ore bodies. The upper edge of the ore-bearing zone is located at a depth of 400 m, and its lower edge was intersected at a depth of 1300 m from the day surface. The conditions of ore localization were determined using structural–geological and petrophysical studies coupled with numerical modeling of the effects of gravitational body forces at purely elastic and postcritical elastoplastic deformational stages. The dynamics of the tectonic stress field in the rock massif was reconstructed using the results of mapping of morphogenetic and kinematic characteristics of fault and fracture systems, as well as data on petrography and mineralogy of rocks and vein-filling material. It was shown that the fault framework of the deposit was formed in four tectonic stages, three of which took place in the geologic past and one of which reflects recent geologic history. Each tectonic stage was characterized by different parameters of the tectonic stress–strain field, fault kinematics, and conditions of mineral formation. The following types of metasomatic rocks are recognized within the deposit: high-temperature K-feldspar rocks and albitites (formed during the Late Paleozoic as the primary structural elements of a granitic massif) and Late Mesozoic low-temperature preore (hydromicatized rocks), synore (hematite, albite, chlorite, and quartz) and postore (kaolinite–smectite) rocks. The following petrophysical parameters were determined for all rock types: density, effective porosity, wet- and dry-rock shear (S-wave), and compressional (P-wave) velocity. Ultrasonic measurements were made to obtain the dynamic Young's modulus, shear modulus, bulk modulus, and Poisson's ratio. The results confirm that all studied lithologies (host granites, K-feldspathized rock with albitites and hydromicatized rocks) have drastically different petrophysical parameters. These values were used as the basis for tectonophysical modeling of Late Mesozoic synore deformation induced by gravitational forces. It was shown that the domains of most intense deformation are confined to the intersections of submeridional fluid-conducting faults with sublatitudinal K-feldspathized and albitized zones, which acted as concentrators of external induced stresses. The formation of enriched ore shoots at these structural nodes can be explained by the suction-pumping of ore-forming fluids by pipe-like (tubular) conduits under oriented stress. The deformation of K-feldsparthic rocks and albitites under stresses exceeding the elastic limit raised their fracture permeability due to cataclasis and brecciation and created favorable conditions for circulation of mineralizing fluids and precipitation of minerals. The use of tectonophysical modeling for the reconstruction of paleotectonic and fluid flow conditions during formation of hydrothermal mineralization allows a more precise evaluation of ore potential in deep levels and flanks of ore deposits.

DOI: 10.1134/S1075701515040030

INTRODUCTION

The main goal of this study is to investigate the mechanisms and processes involved in the formation of hydrothermal ore deposits in fault-fracture zones during changing stress–strain conditions within a crystalline rock massif at different tectonic stages. This formulation of the goal is based on the underlying definition of tectonophysics as a study the mechanisms generating deformational structures in the Earth's crust, which involves a wide range of applied tasks, including prospecting, exploration, and mining of mineral deposits (Gzovskii, 1975).

The Antei Mo–U deposit (Fig. 1) was chosen as an object of this study because its underground infra-

Corresponding author: V.A. Petrov. E-mail: vlad@igem.ru

structure provides information for the entire set of geomechanical surveys being conducted in an underground research laboratory for geodynamics (Laverov et al., 2008; Rasskazov et al., 2012; Shchukin et al., 2015).

At the same time, the Antei deposit is a unique object for tectonophysical reconstruction of stress conditions during the formation of hydrothermal mineralization in the geological past using the combination of modern structural, petrophysical, and tectonophysical methods, including the quantitative estimates of tectonic stresses and deformations. The proposed approach can be described as a paleotectonophysical analysis of conditions of hydrothermal ore formation.

The tectonic stress field acting in a real geological medium is very heterogeneous and always varies in the values of the acting stresses and the orientation of the normal principal tectonic stresses. Depending on the scale of the studies and used methodology, there can be different ranks of stress fields related to the effects of different, hierarchically structured, factors. There is a direct and inverse relationship between tectonic stress fields, rock deformation, and tectonic motions. Therefore, the description of structural heterogeneities and analysis of deformations will require ranking of the stress fields, which provided a spatiotemporal framework for the functioning of a tectonodynamic system. The term "tectonodynamic system" was first used by Nikolaev (1992) to describe a combination of stresses acting on a statistically homogeneous medium and deformation mechanisms manifested in this medium via tectonic motions. This gives rise to the formation of a structural paragenesis manifested by stable and ordered assemblies of genetically related brittle (faulting) and ductile (folding) deformations of the same rank, which developed in close spatial and temporal proximity in the stress field of an appropriate scale.

The formation of structural parageneses in tectonodynamic systems depends upon the petrophysical properties of rocks and the strain rate, which is a function of the amount of energy released from deformation during dynamic metamorphism per unit time (specific strain energy dissipation capacity). This idea was laid as a basis for the strain–velocity concept of formation and typification of ore deposits (Starostin, 1994).

Based on the overall goal of the study, the following specific objectives were identified to investigate hierarchically structured tectonodynamic systems such as ore deposits: (1) detailed structural–geological mapping in underground mines, petrographic and mineralogical analysis of drill cores, (2) genetic analysis of regional and local stress fields, (3) identification of structural hierarchy of the rock massifs, (4) determination of primary and secondary deformation mechanisms, (5) identification of heterogeneity of structural, mineralogical, chemical, and petrophysical characteristics of the rocks, and (6) determination of changes in the rock properties at different PT conditions, grades of water saturation, and the duration of deformation.

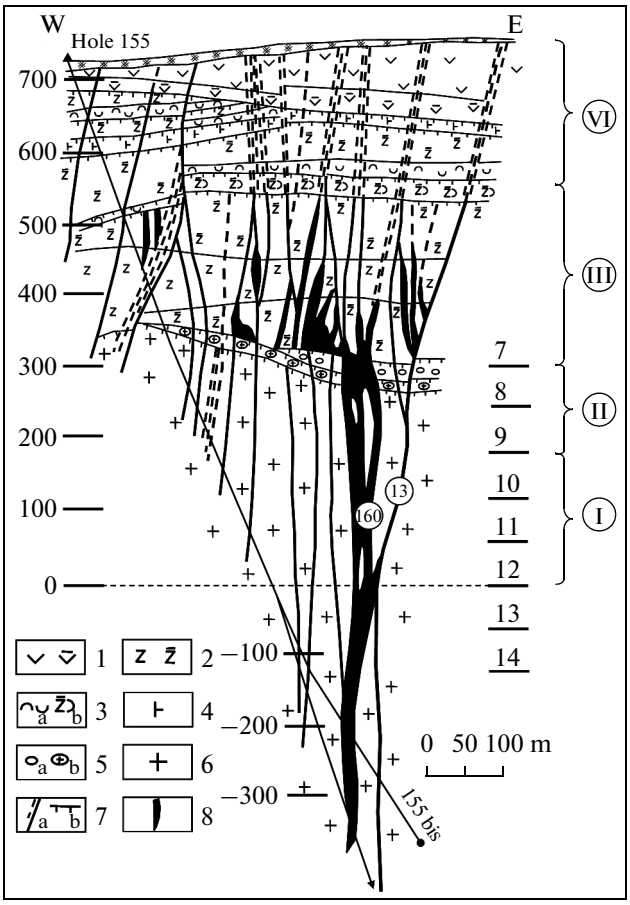

Fig. 1. Geological cross-section across the Antei deposit, after Ishchukova (2007). (1) felsite, (2) trachydacite, (3) trachydacitic tuff (a) and tuff lava (b), (4) basalt, (5) conglomerate (a) and residual granitic material (b), (6) granitic rock, (7) steeply dipping fault (a) and gently dipping detachment (b), (8) ore zones and ore bodies. The ore bodies of the central site of the Strel'tsovskoe deposit localized in the volcanosedimentary caldera fill are situated above faults 160 and 13. The scale of height above sea level is given to the left, the numbers and location of underground working levels within the section are given to the right. The main layer (I) and additional (II–IV) layers of the numerical tectonophysical model are shown in brackets (see text for explanation).

Each of the above objectives can be fulfilled by a unique combination of field studies and laboratory experimental methods, which include geological mapping and zonation, tectnophysical analysis of stress fields, tectonic motions and deformations (Gzovskii, 1975; Gushchenko, 1979; Angelier, 1984; Etchecopar, Mattauer, 1988; Sim, 1991), structural–petrophysical (Starostin, 1979, 1988), microstructural (Lukin et al., 1965), petrographic and chemical analysis of minerals, characterization of pore space morphology, etc.

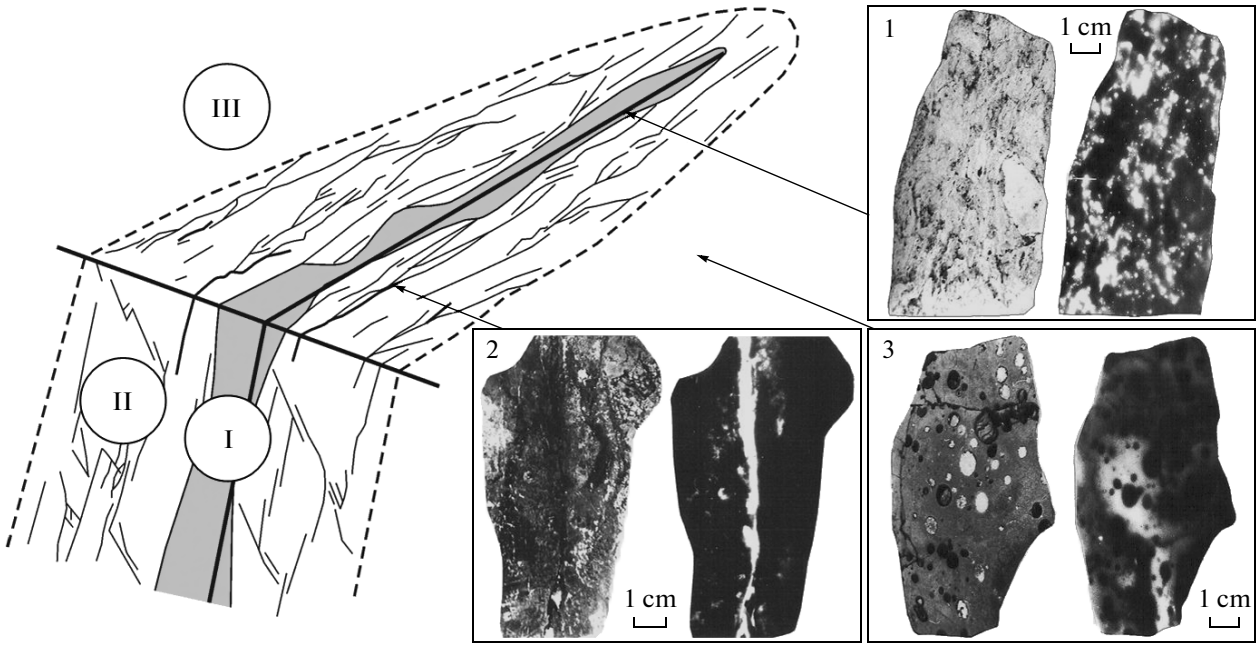

Fig. 2. A conceptual model of fault zone internal structure, after Shipton and Cowie (2003). (I) Central part (core) of the fault with the principal fault plane and intensely deformed rocks (gouge, mylonites, cataclastites, breccias), (II) zone of dynamic influence (failure) intensely dissected by shear fractures and tensile cracks, veins, and veinlets, (III) intact host rock (protolith). Photographs and autoradiographs show examples of morphological types of uranium-bearing aggregates: (1) disseminated mineralization in the fault core, (2) a veinlet in the zone of dynamic influence, (3) veil flash within the weakly fractured protolith.

The use of GIS and CAD systems for processing geological–geophysical, mineralogical, petrographic, geochemical, structural, and other data is of particular importance for computer-generated modeling of orebodies and ore-forming processes (Petrov et al., 2015). This allows the visualization of 3D geologic models in a hierarchical geological medium and numerical modeling of deformation, filtration, thermal and other processes.

METHODS

The results of geostructural, petrophysical, and tectonophysical studies were used to reconstruct conditions of hydrothermal mineralization within a nonstationary stress field.

Geostructural Studies

The modeling and 3D visualization of tectonic deformations and a deposit-scale fault network require the unification of the available structural and geological data on the morphology, internal structure, and spatiotemporal relationships of faults, fractures, veins, veinlets, etc. For this purpose, it is most expedient to use an approach proposed by Marrett and Peacock (1999), which comprises geometric, kinematic, and dynamic analyses.

Geometric analysis is the description of locations, shapes, sizes, and orientations of faults of diverse morphology and structure. Large faults, as a rule, consist of a series of coplanar, closely spaced sutures accompanied by their own zones of fracturing and disintegration, shearing, crushing, and brecciation that are arranged en echelon in selvages of fault planes. Such a pattern hampers interpretation of structural data and their coordination with results of mineralogical, geochemical, petrophysical, tectonophysical, geophysical, and other investigations. Thus, in the description of the architecture of each complexly structured fault zone, the central part (core), the zone of the dynamic effect (failure), and intact wall rock (protolith) are recognized (Fig. 2).

Such a model of the spatial relationships and hierarchy of various elements of the internal structure of a fault zone is accepted as a basis for description of the mineral and chemical composition, character, and degree of hydrothermal–metasomatic alteration, and petrophysical parameters of rocks (porosity and permeability, density, stress–strain properties, thermal conductivity, etc.).

Since the fault framework can be modified under the effect of stresses manifested by deformations and displacements, *kinematic analysis* addresses the morphogenetic characteristics of faults that produce different types of displacement (strike slip, normal, or reverse faults) and directions of motions at different tectonic stages. The attitude, morphology, and age of slickenside indicators such as striations and grooves on the fault plane are used for this purpose. Coeval tec-

tonodynamic systems are recognized based on the relationships between genetically conjugated tension cracks and shears (Rastsvetaev, 1987; Nikolaev, 1992; Seminskii, 2003). The different orientations and amplitudes of dislocations in various tectonodynamic systems reflect different stages of faulting. Fault kinematic analysis is part of tectonophysical studies, which address the stress distribution, faulting and deformation structures as well as the development of the fault-block structure of rocks.

Dynamic analysis is used to describe the deformation behavior of rocks in the stress field. It is difficult to constrain the rheology of rocks during tectonic events, although these data are needed for the reconstruction of pathways and conditions for the migration of ore-bearing fluids (Oliver et al., 2001). Dynamic analysis interprets the spatial structural patterns of rocks and minerals (quartz, feldspar, calcite) as indicators of deformation. The deformation behavior of rocks is predicted based on their physicomechanical (petrophysical) parameters (density, porosity, elasticity, strength, etc.).

Petrophysical studies

The following petrophysical parameters were determined in this study: density (ρ, g/cm^3), effective porosity (Π, %), wet- and dry-rock shear (S-wave), and compressional (P-wave) velocity (V, km/s). Ultrasonic measurements were made to obtain the dynamic Young's modulus (E, GPa), shear modulus (G, GPa), bulk modulus (K, GPa), Poisson's ratio (μ).

Petrophysical analysis was performed on oriented core samples collected underground from mine drives. The samples were cut into cube (~50 mm long), duplicate (for determination of V_P and V_S), prism-shaped subsamples (10 mm thick, for determination of ρ and Π), and thin section (usually oriented) for mineralogical and petrographic analyses. The directions north and east were labeled as the x- and y-axes, respectively, and the vertical direction as the z-axis. The orientation of samples is used to determine the anisotropy of rock physical properties, like density, porosity, permeability and strain–stress relationships.

Density and effective porosity were measured by hydrostatic weighing of each sample dry and water saturated (partially or completely). The samples were weighed once dry with accuracy of 10 mg then were totally immersed in water and weighted after 1 min, 10 min, 1 h, 10 h, 1 day, 3 days, etc. until complete saturation with water was achieved. The calculations were done using the following formulas (Burmistrov et al., 2009):

$$\rho\ (\text{g/cm}^3) = 0.998 \times \text{Pd}/(\text{Pd} - \text{Pfs}), \quad (1)$$

$$\Pi\ (\%) = 100 \times (\text{Pfs} - \text{Pdw})/\text{Pd} - \text{Pfs}), \quad (2)$$

where Pd is the weight of dry sample in air, Pdw is the weight of dry sample in water, Pfs is the weight of fully saturated sample in water.

The density determined by this method corresponds approximately to the density of a solid phase or a mineral density of the rock. Given a large volume of closed pore, it may differ considerably from true mineral density but this difference is in general relatively small. The uncertainty in density measurements is reduced with increased sample volume.

The uncertainty in Π measurements is also reduced with increasing volume of the sample. For example, for the sample volume of 200 cm^3 given the weighing accuracy of $\Delta P = 0.01$ g, Π will be equal to 0.01%. Porosity measurements on small volume samples are usually accurate to a few tenths of a percent. The porosity of a rock sample does not affect the accuracy of measurements, which can be increased by increasing the accuracy of weighing scales.

The elastic parameters such as P-wave (V_P) and S-wave (V_S) velocities were determined on dry and water-saturated rock samples using a set of equipment consisting of a Panametrics PR5072 (USA) ultrasonic pulser-receiver unit connected to two 1-MHz P- and S-wave transducers (Panametrics V101 and Panametrics V151, respectively). The signals received were digitized using a TiePie508 (Netherland) oscilloscope. Polysaccharide gel was used as ultrasonic couplant. The wave velocities were measured on a dry sample after drying at 70°C for 4 h and on a water-saturated sample after sequential immersion in water for 7 days. Unlike vacuum water impregnation, this method allows complete water saturation to be achieved in low-porosity samples. Uncertainties in the V_P and V_S measurements after calibration with the quartz and steel standards were not less than 1%.

From ultrasonic testing of dry and water-saturated samples, the velocities of P-wave (V_P) and S-wave (V_S) were plotted along three orthogonal directions and the elliptical diagram of wave distribution on each plane was constructed. These diagrams display anisotropy of V_P and V_S in both states of the rock. For example, velocities increase in all directions and the anisotropy of elastic properties is not present if the microfractures or mineral grains are distributed uniformly through the rock sample. An increase in V_P and V_S in a particular direction during water saturation (pronounced anisotropy) is associated with the preferred orientation (elongation) of mineral aggregates, the presence of open linear channels along the intergrain boundaries and/or an oriented system of open (water-conducting) microfractures. Such a directional pattern is commonly caused by stress exceeding the long-term rock strength and leading to brittle and ductile deformations.

The dynamic Young's modulus (E, GPa), shear modulus (G, GPa), bulk modulus (K, GPa), and Pois-

son's ratio (μ) were computed by the following formulas (Burmistrov et al., 2009):

$$E = \rho V_S^2 (3V_P^2 - 4V_S^2) / 2(V_P^2 - V_S^2), \quad (3)$$

$$G = \rho V_S^2, \quad (4)$$

$$K = \rho(V_P^2 - 4/3 V_S^2), \quad (5)$$

$$\mu = (V_P^2 - 2V_S^2)/2(V_P^2 - V_S^2), \quad (6)$$

where ρ is the rock density (g/cm^3), V_P is the P-wave velocity (km/s), V_S is the S-wave velocity (km/s).

The measurement of petrophysical parameters coupled with structural studies and mineralogical–petrographical analysis of rocks provide the information required for tectonophysical numerical modeling.

Tectonophysical Modeling

The study on possible mechanisms responsible for the generation of tectonic stresses and establishment of the stress regime at the Antei deposit was performed through finite-element numerical modeling, which was accomplished using the UWay program developed at the Institute of Applied Mechanics, Russian Academy of Sciences (Vlasov et al., 2004).

To calculate the stress fields in a geological medium it is necessary to construct a *numerical model*, which in turn integrates three models:

a *geometric model* of the geologic body consisting of conjugate 2D or 3D elements (depending on the type of problem to be solved) of varying sizes and geometries;

a *rheological model*, in which 2D or 3D elements are attributed different elastic and strength properties;

and a *internal force model*, which determines the loading and motion conditions at the outer and inner boundaries of the geometric model, as well as the effects of the distributed body forces or temperature field (for thermoelasticity problems).

These three models are built in several stages and usually require adaptation where data on a natural object are compared to calculated values. The model's adaptation envisions a reasonable compromise between the simulator's wish to consider as many structural parameters of the object as possible, the simulator's ability to convert a complex geological object into a digitized format and the capabilities of applied software. Because of unavoidable errors, fairly complex 3D models are built by adding incrementally sophistication to all three models (geometry, properties, and forces). Identification of errors in integrated models is often a time-consuming process. Therefore, subdivision into smaller computational subdomains is used, which are successively added to by the remaining fragments of the geometric model. Boundary conditions at the outer boundaries of the geological object are set by extending the geometric model to minimize boundary condition effects, e.g., stress concentration, which is absent in an infinitely large volume. Most of the modeling time (up to 95%) is spent building a geometric model of the object.

RESULTS AND DISCUSSION

Geostructural Analysis

Mineralization at the Antei deposit consists of steeply dipping vein and stockwork ore bodies associated with splays of the NNE–SSW-trending Central fault zone containing a wide (up to a few tens of meters) zone of dynamic effect (Laverov et al., 2008; Petrov et al., 2009). Studies were performed at hypsometric levels 9–14 of the Antei deposit located at depths ranging from 550 to 870 m below the surface. Oriented samples of host rocks were taken from each type of host rock at all horizons studied.

The major elements of the fault network are closely spaced, subparallel fault zones 160 and 13 and auxiliary faults 161 and 160d splaying from the main fault 160. Faults 160, 161, and 160d are splays of fault 13 at its hanging wall.

Fault zone 160 (the major ore-controlling structure) consists of 1–3 subparallel sutures striking mostly NNE–SSW (25°–30°) and dipping at high angles (75°–85°) to the ESE, which evolved at the postore stage into a dextral en echelon shear array. Based on the structural position of coeval fault-hosted veins, the cumulative horizontal offset may reach several meters. Sutures filled with clay-rich gouge packets up to 0.5 m thick are accompanied by intensely deformed zones reaching up to a few meters in thickness. Fault 160 is sealed upward by low-angle detachment faults at the unconformity between the prevolcanic basement and the Streltsovskaya caldera volcanic fill.

Fault zone 13 is also composed of several NNE–SSW-trending en echelon sutures dipping at high angles (75°–80°) to the WNW. This fault displaces the contact between basement and caldera fill for up to 12 m, cutting the volcanic units and is traced at the surface. The morphology and mineralogy of the sutures suggest that they were formed at the late stages of hydrothermal activity, as indicated by the presence of laterally persistent postore veins and veinlets. It can be thus assumed that both strike-slip and normal faulting took place along this fault zone at the end of hydrothermal activity. The presence of late, postore quarz-bearing veins forming subparallel, en echelon arrays at levels 13 and 14 is interpreted as a direct evidence for an extensional regime (normal faulting). Faults 160 and 13, having the same strike but opposite dip, merge below level 12. This results in the formation of a tectonic wedge, a zone of intense fracturing bounded by faults 160 and 13.

In fault zones 160 and 13, each suture is accompanied by zones of fracturing and disintegration, crushing and brecciation that developed en echelon in sel-

vages of tectonic planes. Thus, the central part (core), the zone of its dynamic effect (failure), and intact wall rock (protolith) are recognized in each fault zone. Data on mineralogy, geochemistry, metasomatism, and petrophysics are tied to this basic model.

The background fracturing in the granitic rocks is formed by a system of high- to low-angle (15°–35°) fractures striking NE–SW, NW–SE, E–W and N–S. Statistical analysis showed that the main fracture sets have become misoriented depending on the hypsometric level. The EW-trending (275°–285°) fracture set is best expressed at level 9. This system is documented at level 11 as well, but the leading role belongs here to the NW–SE (320°–340°) trend. It is interesting to note that irrespective of the hypsometric level, the highest fracture intersection density defines several zones trending ENE–WSW along the strike of Late Paleozoic K-feldspar–albite metasomatic bodies. The influence of these vein-like bodies on localization of ore shoots is discussed below.

Delineation of metasomatic rocks in ore deposits based on field and thin section evidence allowed the following types of metasomatic rocks to be recognized: Late Paleozoic high-temperature (K-feldspar rocks and albitites) and Late Mesozoic low-temperature preore (hydromica), synore (hematite, albite, chlorite, and quartz) and postore (kaolinite–smectite). The predominant low-temperature metasomatic rocks are controlled by fault zones 160 and 13, a set of subparallel faults (160d and 161) and a set of minor fractures.

The age of high-temperature K-feldspathic and albititic rocks is defined by the Undinsky host granites, which have an emplacement age of 254–245 Ma (*Geologicheskoe* ..., 1997), corresponding to the Late Permian–Early Triassic. K–Ar dating of mica from low-temperature preore hydromica alteration zones in granites yielded ages in the broad range 138 ± 6 to 129 ± 5 Ma (Andreeva et al., 1996). Economic Mo–U mineralization is interpreted to have formed at 136 ± 3 Ma (Chernyshev and Golubev, 1996; Golubev, 2011). The preore hydromica alteration and Mo–U mineralization are considered to be Late Jurassic–Early Cretaceous in age.

The spatial distribution of high-temperature K-feldspathic and albititic alteration aureoles (hereinafter referred to as K-feldspar rocks and albitites) is characterized by several distinct trends. The vein-like bodies of metasomatic rocks are traced in the ENE–WSW direction (hereinafter referred to as sublatitudinal) diagonal to the strike of the NNE–SSW (hereinafter referred to as sublongitudinal) ore-controlling faults. The bodies of K-feldspar-rich rocks vary in thickness from a few centimeters to few meters. They are not satisfactorily traced by mapping but can be delineated from detailed mineralogical, petrographic, and geochemical studies.

The alteration is expressed in development of numerous microcline porphyroblasts a few centimeters in size, which are much larger than the grains of the Late Paleozoic host granites. The intensity of alteration is marked by bands of gray or milk white quartz up to a few decimeters in size. The later albitites are present within the feldspathized zone. Albite commonly occurs as finely twinned tabular grains at the rims of K-feldspar and plagioclase grains. With increasing intensity of metasomatic alteration, the albite rim gradually widens, replacing earlier feldspars, and the rock tends to have light grey to white color, a sugary appearance and may contain up to 10 wt % Na_2O. Sublatitudinal bodies of high-temperature K-feldspar rocks and albitites representing the primary structural elements of a granitic massif are the products of metamagmatic alteration, which took place during the late stages of crystallization of granitic magma before its complete solidification.

Late Mesozoic metasomatic rocks are spatially associated with two large structural elements acting as flow conduits, the main ore-bearing fault 160 and fault 13. Since fresh, unaltered granites seem to be almost absent, they have only conventional boundaries delineated at each level. Some varieties contain relics of biotite, although minor amounts of newly formed hydromica (up to 1.5%), carbonate and quartz are also present. Preore hydromica alteration phases with established alteration zoning patterns are widespread at all levels (Andreeva and Golovin, 1998). Hydromica alteration aureoles vary in thickness from a few meters (around occasional fractures) to 50–70 m. They contain the inner, most intensely altered zones (in which hydromica, carbonates, and quartz account for up to 50% of the total volume of the rock) up to a few meters thick.

The reconstruction of the dynamics of the tectonic stress field in the rock massif shows that the fault framework of the deposit was formed in four stages, three of which took place in the geologic past (Fig. 3), and one of which reflects recent geologic history. These four stages are marked by a reorientation of the principal normal stress and shear stress axes, changes in the stress–strain state of rocks, changes in the direction of fault displacement, and changes in the tectonophysical conditions of ore formation and location.

The first stage of tectogenesis is reconstructed from the lineation of preore high-temperature feldspathized and albitized rocks, which probably indicates a sublatitudinal orientation of the maximum compressive stress axis (σ_1, positive values, i.e., $\sigma_1 \geq \sigma_2 \geq \sigma_3$). Such orientation is reconstructed for the Variscan (Late Paleozoic) tectonic events in this part of Eastern Transbaikalia (Petrov, 2007). Analysis of geological and geophysical data shows that the sublatitudinal zones of high-temperature metasomatism at the Antei deposit reflect structural heterogeneities in the crystalline basement, which define the position of the long-

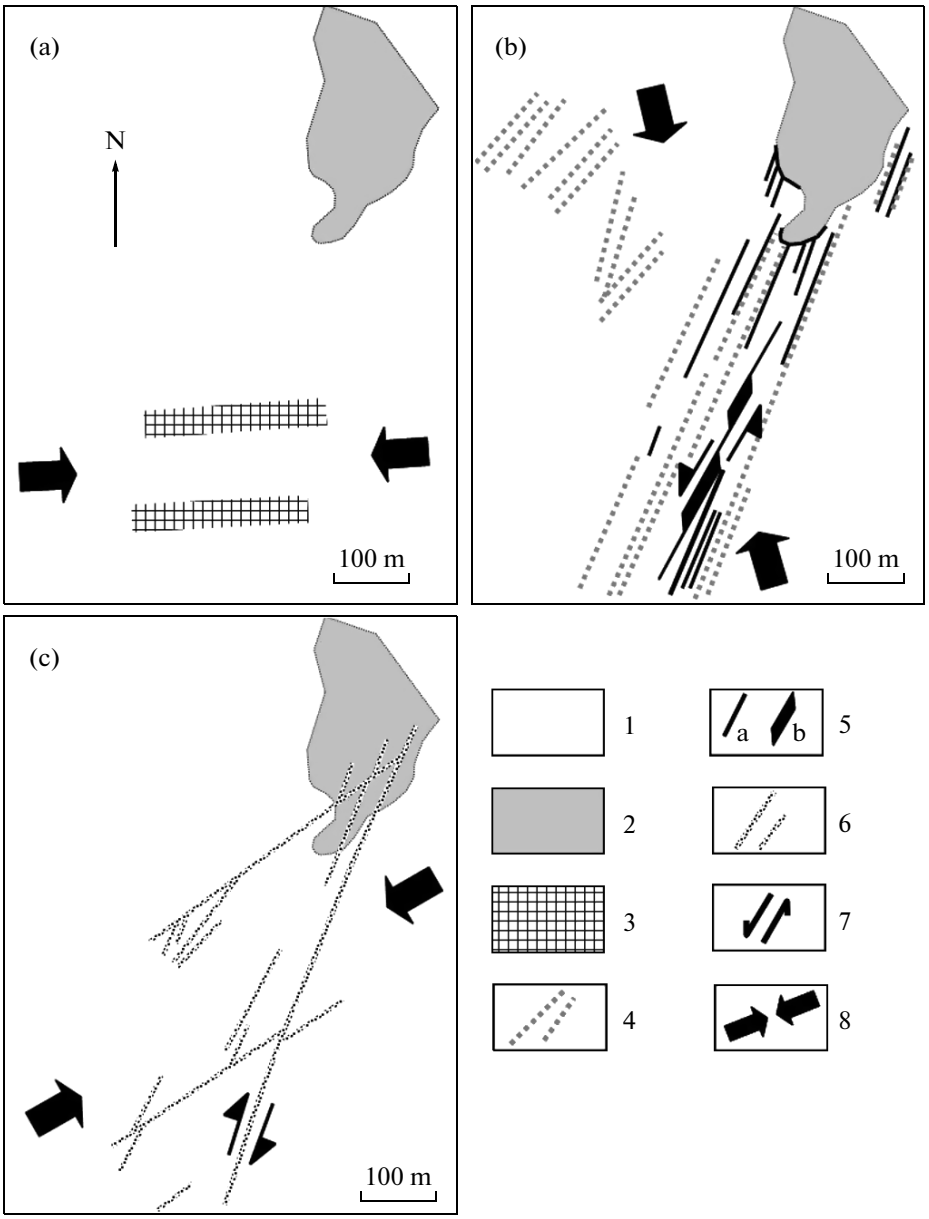

Fig. 3. Reconstructed orientations of principal compressive stresses during the main tectonic stages (at level 10). (a) Late Paleozoic high-temperature metasomatites (K-feldspathized rocks and albitites), (b) Late Mesozoic preore hydromicatization and synore hematite–albite alteration, (c) postore argillization (kaolinite, smectite). (1) Granites, (2) basal conglomerate, (3) K-feldspathized rocks and albitites, (4) hydromicatized rocks, (5) albite–hematite alteration (a) and ore bodies (b), (6) postore mineralization, (7) direction of motions along the fault planes, (8) direction of maximum compressive stress. Arrow shows the direction of north (N).

lived Argun tectonomagmatic zone (Ishchukova et al., 2007) within the Streltsovskaya caldera.

The second stage comprises preore hydromica alteration, synore hematite–albite–chlorite alteration and ore formation processes. Based on the morphology of orebodies (Atlas ..., 1982) and kinematics of ore-controlling faults, the NNW–SSE orientation of maximum compressive stress axis σ_1 at this stage demonstrates that sinistral motions occurred along fault zone 160. This resulted in the formation of fault-bounded pull-apart structures at releasing bends, which were sequentially filled with uranium-bearing material. Low-amplitude tectonic movements at this stage were concentrated around fault 160, whereas fault 13 resided within its stress shadow and was thus inactive.

The spatial position of ore shoots is defined by the intersections of sublatitudinal bodies of high-temperature metasomatic rocks with the submeridional fault zone 160. The formation of enriched ore shoots can be explained by suction-pumping of ore-forming fluids

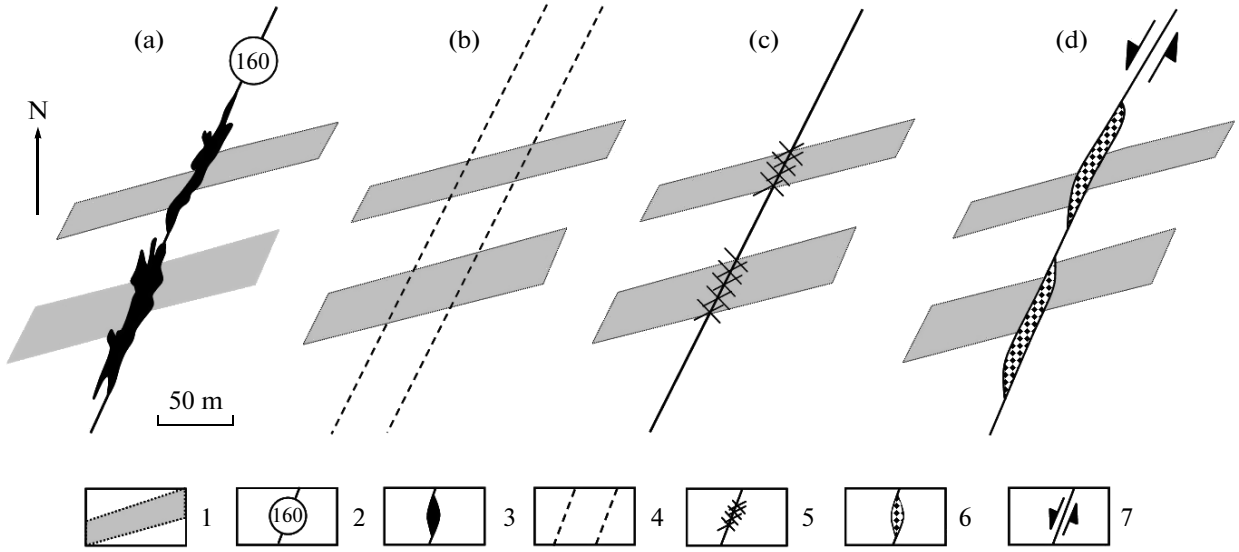

Fig. 4. Model of formation of ore shoots at the intersections of K-feldspathized and albitized veins with ore-controlling fault 160: (a) section of level 10 with outlines of orebodies based on exploration and mining data, (b) the inception of a Late Paleozoic submeridional zone of heteroneity orthogonal to sublatitudinal bodies of K-feldspathized rocks and albitites, (c) formation of zones of intensely deformed rocks at the intersections of the principal plane of fault 160 with brittle K-feldspathized rocks and albitites, (d) tectonic motions (sinistral faulting) and formation of pull-apart structures and their filling with ore material. (1) Vein-like bodies of K-feldspathized rocks and albitites, (2) plane of fault 160, (3) ore bodies, (4) near-fault zone of heterogeneity, (5) zone of intense fracturing, (6) pull-apart structures, (7) direction of motion along the fault plane. Arrow shows the direction of north (N).

by pipe-like (tubular) conduits under oriented stress. The mechanism of suction-pumping of ore-forming fluids into drainage conduits was discussed in detail elsewhere (Dykhuizen, 1992; Nordqvist et al., 1996 and others). It was shown that fluid conduits may develop along dilational fault segments, thus enhancing the directional permeability toward the intermediate stress axis (σ_2). Those faults most prone to reactivation, hydraulic fracturing and/or infiltration of ore-forming fluids tend to be confined to the axis lying in the $\sigma_1\sigma_2$ plane (Sibson, 1996; Cox, 2005). The possibility of these processes to occur is then dictated by the magnitude of differential and shear stresses, pore fluid pressure, temperature regime, petrophysical properties (tensile strength, friction coefficient, and angle of internal friction), rate and kind of deformation, and orientation of faults with respect to the stress field (Cowie, 1998).

The application of a differential stress produces brittle deformation in elastolasting K-feldspathized and albitized rocks. As a result, conditions at the intersections between K-feldspathic and albititic alteration zones and fault 160 were particularly favorable for the circulation of ore-forming fluids and ore deposition. The sequence of ore-shoot formation is shown in Fig. 4.

Proper understanding of the tectonophysical conditions of ore formation in fault-fracture structures of the Antei deposit requires full answers to critical questions such as the effects of temperature and pressure, as well as the structure-forming role of fluid flow. This information is important for setting boundary conditions and values of effective parameters, e.g., parameters of plasticity.

Hydrothermal uranium ore deposits are through to have formed at temperatures of 180–140°C under near-isothermal conditions. The solutions have in general high CO_2 contents (from $n \times 10^2$ to $n \times 10$ g/kg H_2O), decreasing from the lower to upper levels and from early to late mineral assemblages (Mironenko, 1985; Naumov et al., 1985). At the same time, the seismotectonic movements along flanks of the host faults may have created local zones with anomalously high temperatures and pressures. It was shown that short-term (few-second) coseismic slip at a rate of the order of 1 m/s induces a local increase in temperature of up to 750–1600°C and higher at fault contact surfaces, which is accompanied by melting and the formation of pseudotachylytes (Boullier et al., 2001; Di Toro et al., 2005; Tagami, 2012). Seismotectonic activity in shear zones may account for high temperatures (530–300°C) determined for uranium ore-forming processes (Aleshin et al., 2007).

The microstructural and thermobarogeochemical data on planar concentrations of fluid inclusions in different quartz generations demonstrate that the uranium mineralization stage was characterized by preferential entrapment of inclusions with homogenization temperatures of 220–160°C and salinities of 2–7 wt % NaCl eq. (Petrov et al., 2013). The presence of a differently oriented planar system in the ore cluster suggests that extensional shear (hydraulic extension fracturing) took place in zones of weakness during ore

formation. A tectonophysical model of this mechanism was given by Cox (2005). In particular, the results show a correlation between deformations, variations in fluid pressure (pore–fluid factor, λ_V), and conditions of migration of mineralizing fluids in crust composed of alternating low- and high-permeability horizons. Fluid flow in low-permeability zones (barriers) creates an overpressured hydrothermal regime (supralithostatic fluid pressure, $\lambda_V > 1.0$) in their lower part, which is manifested in hydraulic fracturing of rocks, indicating the structure-forming role of hydrothermal fluids. Dip-slip detachment faults at the basement–sedimentary cover contact and thick horizons of volcanic rocks (basalts, felsites, and trachydacites) acted as barriers to fluid flow at Antei deposit.

Fault zones can function as valves intermittently discharging focused fluids into extension fractures that are optimally oriented in the prevailing stress field (Sibson, 1992; Nguyen et al., 1998). Explanations put forward to account such mechanism include decompression and dilatancy leading to the infiltration of O_2-bearing meteoric waters along faults being carried down into the deeper levels. Such processes are most evident in the seismically active faults (Lin et al., 2003). The fault-valve action that gives rise to infiltration of meteoric water and its mixing with hydrothermal solutions in zones of ore deposition was demonstrated by the example of the Argun deposit (Petrov et al., 2014). At the Antei deposit, fault zone 13 seems likely to serve as fluid conduit for meteoric water. Oxygen and hydrogen isotope data for sericite and illite support the involvement of a meteoric water component along with magmatic fluids in the formation of hydrothermal mineral assemblages (Andreeva and Golovin, 1998). Some additional aspects regarding the structure-forming role of fluids and the role of faults on the fluid heat and mass transfer were discussed in earlier papers (Petrov, 2011; Mal'kovskii and Pek, 2014). The data from these studies are important for reconstruction of paleotectonic setting and fluid infiltration during ore formation at the Antei deposit.

The third stage reflects the rearrangement of the tectonic stress field, when the σ_1 orientation rotated by 45°–50° and the compressive stress trajectories became oriented NE–SW. This stage is marked by the concentration of principal stresses in the areas surrounding fault 13, which had emerged from the stress shadow of fault 160, and by the maximum development of persistent veins filled with postore minerals (quartz, fluorite, kaolinite, smectite) at the end of hydrothermal process. Taking into account the displacement of the contact between the granitic basement and the volcanic cover and the orientation of splays filled with postore mineralization (Fig. 3c), movement along fault 13 can be interpreted as dextral strike-slip, normal strike-slip or oblique-slip.

Thus, the ore-forming process at the Antei deposit took place in a non-stationary stress–strain field and was accompanied by changes in the principal stress directions by 45°–90°.

The fourth (recent) stage has inherited the main features of the preceding stage, when maximal compressive stresses trajectories were oriented in the NE–SW direction. On a regional scale, this is reflected in the strike slip character of the recent stress field (Reinecker et al., 2005; Rasskazov et al., 2014). On the scale of the deposit, the NE–SW direction of compression is reconstructed from the deformation of the initial contours of vertical holes. The study of the deformation of borehole walls, as well as walls of rises and ore passes, is one of the simplest and most exact methods of estimation of the stress axis acting within a rock mass (Hudson et al., 2003). The key point in the structural analysis of the stress field is that the walls are destroyed in sectors located perpendicular to the axis of the maximum horizontal compressive stress (S_H). These data were obtained during examination of the stability of an ore pass dislocated due to a rock burst (Fig. 5).

Detailed examinations in 10 vertical holes (rises) showed that at level 9 S_H is oriented at an angle of 50° with respect to the meridian and at level 12 at an angle of 80°. This indicates reorientation of the S_H axis by 30°, which led to a change in the spatial position of sectors of the underground workings that have been more severely damaged (rock slips, rockfalls, rock bursts). It is evident that the structure of the regional stress field becomes more complicated because of the redistribution of the stresses around the worked-out areas and the formation of unloading zones. The interplay of regional and local stresses and their influence on the geomechanical stability of rocks require additional consideration.

Petrophysical Analysis

Petrophysical analysis of more than 200 rock samples showed (Petrov et al., 2007; Laverov et al., 2008; Petrov et al., 2014) that the lowest values of density and elastic parameters (Young's modulus, shear modulus, and bulk modulus) are characteristic of fault cores (shear planes) where the rocks are affected by intense hydromica and argillic alteration while the highest values of elastic parameters are noted in the silicified core of faults (Fig. 6).

Field observations and modeling results indicate that the widest variations of these parameters are characteristic of the zone of dynamic effect of the fault (Sherman et al., 1983 and others) depending of spatial relationship between various types of metasomatites. This is also typical of fault zones in the Antei deposit. The elastic parameters increase with the transition from altered argillic (smectite, kaolinite, and quartz) and hydromicatized rocks (quartz, illite, carbonate) to silicified varieties (a transition from low-velocity elastoplastic to high-velocity elastofrailty medium)

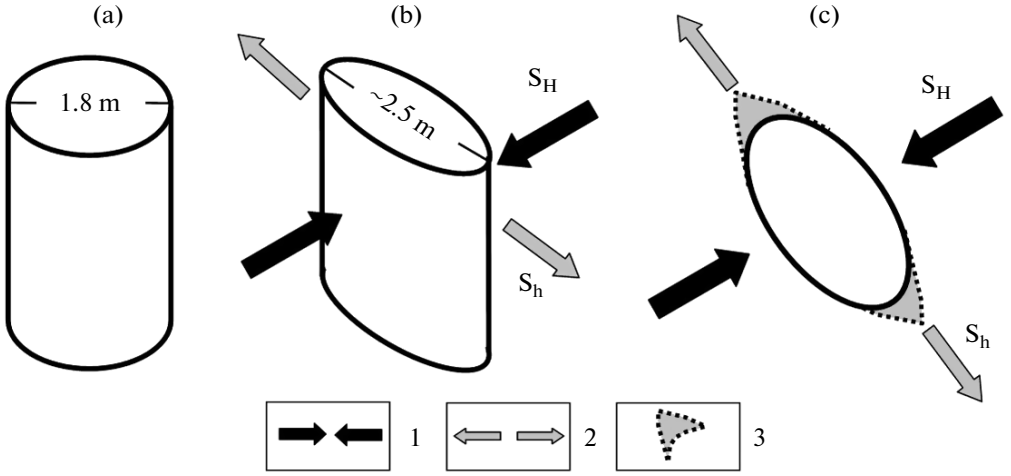

Fig. 5. Reconstructed orientations of horizontal stress axes in the rock massif based on deformation of the walls of a vertical hole at level 9 induced by rock burst in May 2005. (a) Shape before burst, (b) shape after burst, (c) interpretation. (1) Principal (S_H) horizontal stresses, (2) auxiliary (S_h) horizontal stresses, (3) sectors of intense rock fracturing.

(Melosh, 1994). The opposite situation is documented at level 11, where the same parameters decrease in the direction from a silicified core (high-velocity elastofrailty medium) to a low-velocity hydromica and argillic alteration zone.

Uniaxial compressive strength and elastic modulus are highest in silicified rocks and lowest in argillic and hydromicatized varieties (Petrov et al., 2007). A zone of fault-dynamic effect composed of metasomatic rocks of different ages and lithologies is characterized by the greatest variations in the mechanical rock properties. Geomechanical tests indicate that the growth of internal defects and microcracks in rock samples occurs nonlinearly with increasing strain, and the character of failure differs for silicified (burst-like) and hydromicatized and argillic (splitting into sheets and the development of a fracture crack) granite varieties.

Ultrasonic testing of dry and water-saturated samples revealed areas with anisotropic elastic parameters at each level. For example, elevated parameters correspond to sublatitudinal vein-like bodies of Late Paleozoic K-feldspathized and albitized metasomatic rocks, whereas low parameters are spatially associated with the submeridional fault zone hosting uranium mineralization, which is surrounded by a hydromica alteration aureole. At the same time, the low values of elastic parameters are localized in the hanging wall of fault 13 at the deep levels (13–14) of the deposit.

These data support the earlier conclusion (Laverov et al., 2008; Petrov et al., 2009; Petrov et al., 2011) that the general pattern of elastic parameter anisotropy of the massif is controlled by the northern, central, and southern sublatitudinal zones. The northern and southern zones are characterized by elevated P- and S-wave velocities in water-saturated samples in the NE–SW direction, while in the central zone, the velocities increase in the NW–SE direction. The central zone is gradually shifted toward the south with depth, which is consistent with a general southern dip of K-feldspar–albitite veins.

A comparison of data indicates that the nature of elastic parameters anisotropy is controlled by the sublatitudinal orientation of feldpathized and albitized rock bodies, which were formed during the Late Paleozoic as the primary structural elements of the granitoid massif, a heterogeneous distribution of stress and strain in rocks caused by shear displacements along coplanar fault 13 and 160 zones in the Mesozoic, and the present-day stress–strain state of the massif.

These factors are assumed to combine. Mineralogical, petrographic, structural, and petrophysical studies indicate a direct correlation between elastic wave velocities and residual stresses, manifested in the linear (directive) texture of rock samples. The elastic wave velocity tensor, texture of rocks, and orientation of fluid-conducting microfractures are interrelated as well. Trends in elastic anisotropy should be taken into account in determination of the criteria of rock failure.

Modeling of the deformation behavior of the rock massif within the deposit requires formulation of the objective boundary conditions for each petrophysical parameter. The above results suggest that the dominant host lithologies of the deposit are unaltered Late Paleozoic granites, Late Paleozoic high-temperature K-feldspathized and albitized rocks, and Late Mesozoic low-temperature hydromicatized metasomatic rocks. Table 1 shows the average values of petrophysical properties of the main rock types used in the calculation of the rock rheology.

Tectonophysical Modeling

The numerical modeling of deformations using a digital model consisting of geometric, rheological and

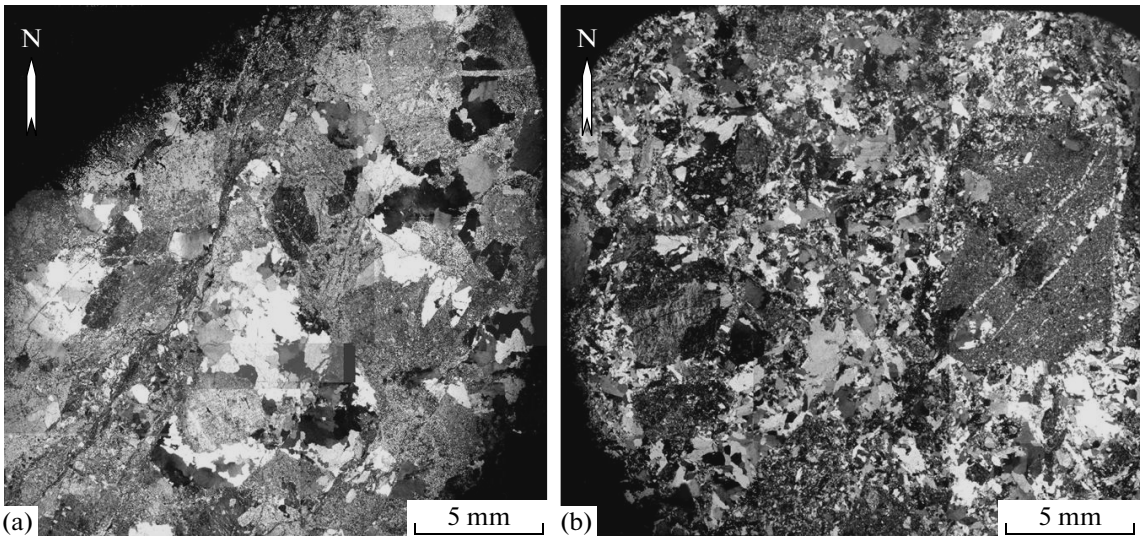

Fig. 6. Digital photomosaics of oriented thin sections A9-0 (a) and A11-0 (b) reflecting different degree of rock alteration in the core of fault 13 at levels 9 and 11. Under crossed nicols. Sample A9-0 is dominated by hydromicatized veinlets ($\rho = 2.58$, $\Pi = 3.2$, $V_P = 4.84$, $V_S = 2.97$, E = 54.7, G = 22.9). Sample A11-0 exhibit intense bulk silicification of the matrix ($\rho = 2.63$, $\Pi = 1.1$, $V_P = 5.68$, $V_S = 3.47$, E = 76.2, G = 31.6). Parameters: ρ is the density (g/cm^3), Π is the effective porosity (%), V_P is the mean P-wave velocity (km/s), V_S is the mean S-wave velocity (km/s), E is the Young's modulus (GPa), G is the shear modulus (GPa).

internal force models represents the third element of tectonophysical reconstruction of hydrothermal ore formation at the Antei deposit during the Late Mesozoic.

Geometric model. Figure 7 shows a simplified 3D fault-and-block model of metasomatic rocks in the lower part of the deposit, which was built using detailed structural, geological, mineralogical, petrographic, and petrophysical data (Laverov et al., 2008; Petrov et al., 2009).

The openGEO software package (developed at the Federal Institute for Geosciences and Natural Resources, Germany) was used for processing initial data with the triangulation method. The model comprises the infrastructure of mine workings; the planes of faults 160, 160d, 161, and 13; and blocks of metasomatic rocks differing in composition, properties, and structural control. In developing the model, we used digitized level plans and sections on a scale of 1 : 500 provided by the geological and mining survey of the Priargunsky Industrial Mining and Chemical Corporation. The new 3D model allows the successful delineation of ore shoots and helps to develop new views of the structural control of mineralization represented by the intersections of faults with sublatitudinal bodies of K-feldspathic and albititic rocks.

The block under investigation is located at a depth between 568 m (level 9) and 750 m (level 12). The block is overlain by host granites, conglomerates, basalts, tuffs, trachydacite tuff lavas, trachydacites and felsites comprising the Streltsovskaya caldera volcanic fill (Fig. 1).

A geometric model was built in AutoCAD files, in which all main elements of the geological structure were represented in a triangulated mesh (Fig. 8).

The elements of the triangular mesh (triangles) were located on six surfaces of a hexagonal prism outside the fault zone (central part of the model). The planar triangular elements inside the fault zone have variable orientation defining the complexity of the fault internal structure. Depths of the upper and lower faces of a hexagonal prim in AuCAD files correspond

Table 1. Petrophysical properties of the main types of host rocks at the Antei deposit used in tectonophysical modeling

Rock type	Density, g/cm^3	Young's modulus (GPa)	Bulk modulus (GPa)	Shear modulus (GPa)	Poisson's ratio	Uniaxial compressive strength (MPa)
Late Paleozoic host granites	2.51	64	41	26	0.23	210
Late Paleozoic K-feldspathic rocks and albities	2.56	76	46	31	0.21	235
Late Mesozoic hydromicatized rocks	2.46	60	39	24	0.25	185

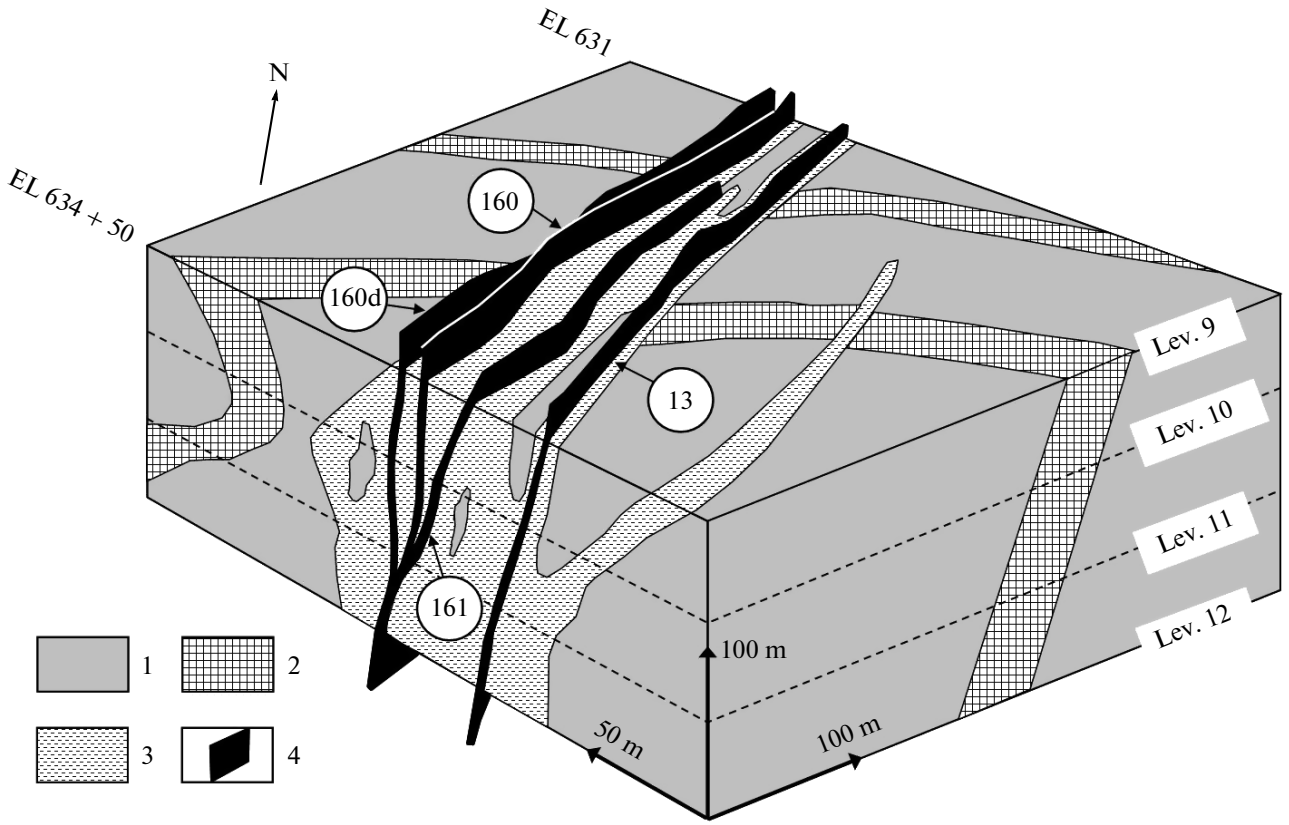

Fig. 7. A simplified 3D model of faults and blocks of metasomatic rocks different in age in the lower portion of the Antei deposit constructed with the OpenGeo software package. (1) Late Paleozoic host granite, (2) Late Paleozoic feldspathized rocks and albitites, (3) Late Mesozoic hydromicatized rocks, (4) fault plane and its number. The vein-like bodies of Late Paleozoic feldspathized rocks and albitites related to prototectonic elements are cut by faults 13, 160, 161, and 160d, which control zones of hydromica alteration, uranium ore bodies, and synore and postore hydrothermal alteration. EL, exploration line, lev., working level. Arrow shows the direction of north (N).

to depths of levels 9 and 12. The long horizontal side of the model (across the strike of the fault zone) was 1000 m and 350 m along the fault zone.

It was assumed originally that a 3D geometric model will be generated using nodes of a triangular mesh. However, a more detailed analysis of the structure of AutoCAD files showed that the triangular mesh was highly heterogeneous and severely distorted, i.e., one side of the triangle was shorter than the other two. Because of the strict requirements on the shape of finite elements (the size of element sides should not differ more than 3–5 times and should preserve the respective degree of detail in the description of a modeled volume), the geometric model was updated by manual tuning. It was taken into account that the 3D geostructural model built in AutoCAD is a hexagonal prism, with upper and lower faces being parallel to the day surface and the remaining four faces vertical. The elements inside this hexagonal prims represent blocks of different lithologies, faults, ore bodies, horizontal and vertical mine workings, and other objects. The model reproduced the following characteristic features: 1) sublatitudinal vein-like bodies of K-feldspathized and albitized rocks dissected by an ore-bearing fault zone; 2) submeridional fault zone (faults 160 and 13) filled with hydromicatized rocks and ore bodies; 3) host granites.

Therefore, the model block was discretized in AutoCAD into two sets of 2D triangles and quadrangles comprising the upper and lower faces of the 3D hexagonal prism. The outer boundaries of the upper and lower faces were converted to a rectangular shape by adding several elements to impose boundary conditions on the vertical faces of the model. Each planar face was comprised of equal number of planar elements (67), including 61 quadratic and 6 triangular. Size of the elements may vary spatially by almost an order of magnitude, but all of them satisfy conditions for simulation. Three-dimensional finite elements were created by merging adjacent nodes of 2D planar elements on these two horizontal faces. As a result we obtained sixty-seven 3D hexa- and pentagonal prisms, which have their upper and lower faces horizontal and their subvertical faces plunging at an angle of more than 45°. This hexagonal parallelepiped forms the core of the computational model for the studied block.

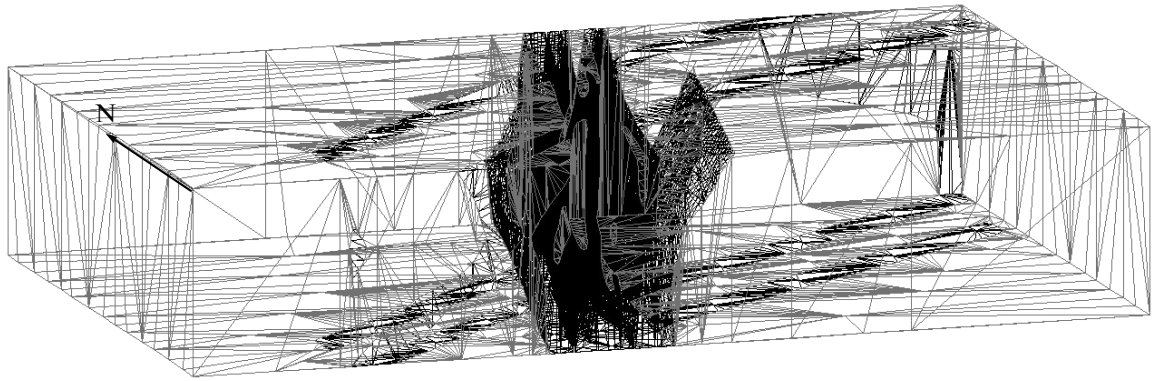

Fig. 8. The lower part of the Antei deposit given as a triangle mesh in axonometric projection (at 60°), which was used as the basis for numerical modeling. Submeridional fault zones traced by late Mesozoic hydromicatized rocks and orthogonal vein-like bodies of Late Paleozoic K-feldspathized rocks and albitites are shown in the central part in black color. Arrow shows the direction of north.

We added 44 three-dimensional elements to the hexagonal prism to remove high stress concentrations (edge effect) from the study area. As a result the model was extended for 350 m along the strike, on both sides of the central part of the fault zone (Fig. 9).

The size of the enlarged model in the horizontal direction was 1000 × 1050 m. The shape of the elements added to enlarge the core of the model was obtained by displacing the nodes along strike of the fault. Thus, the elements used to enlarge the model represent prisms with four strictly vertical faces and two horizontal faces. The rectangular parallelepiped obtained from the core of the model was referred to as the main layer of the digital model for the Antei deposit.

The model required stacking additional layers of the prism in the vertical direction. For this purpose, we used previously published data on the structure of the crystalline basement and volcano–sedimentary cover of the Streltsovskaya caldera (Ishchukova et al., 2007; Laverov et al., 2008). Published data and our observations show that the composition of granitic rocks and fault pattern from level 9 to level 7 are the same as at level 9. Therefore, the top of the model was added with a 120-m-thick layer, with elements similar in plan view to those of the upper face of the main layer. Three-dimensional elements of additional layer 1 have vertical faces similar to those of additional elements of the main layer. The next two layers reflect flat-lying volcanic units, which are similar in their structure to additional layer 1 but differ by the absence of K-feldspathization, albitization, and splays of fault 13 at its hanging wall, as well as by rock thickness and properties considered below.

Therefore, the resulting discrete model of the deposit comprises four layers, the first (main) layer being the lowermost one and the other three being used to extend the model to the day surface. The thicknesses of the layers are 182 m (main), 120 m (first additional), 250 m (second additional), and 200 m (third additional). The model geological medium has a thickness of 752 m and a length of 1050 m and 1000 m across and along the strike of the fault zone, respectively.

The rheological model was built on the basis of the geometric model and the results of structural–petrophysical studies and deformation tests on 200 rock samples collected at the Antei deposit, which were compiled into the database (Shchukin et al., 2015).

The following values of rock properties were taken for host granites of the main layer: rock density of 2510 kg/m^3, Young's modulus of 6.4×10^4 MPa, Poisson's ratio of 0.23; for K-feldspathic rocks and albitites: rock density of 2560 kg/m^3, Young's modulus of 7.6×10^4 MPa, Poisson's ratio of 0.21; and for hydromicatized granites: rock density of 2460 kg/m^3, Young's modulus of 6.0×10^4 MPa, and Poisson's ratio of 0.25. For additional layer 1, which overlies the main layer, the rock properties were taken to be the same as for the main layer. For the overlying trachydacites (additional layer 2) the rock properties were as follows: rock density of 2400 kg/m^3, Young's modulus of 4.0×10^4 MPa, and Poisson's ratio of 0.35. The uppermost felsites (additional layer 3) were assumed to have the rock density of 2400 kg/m^3, Young's modulus of 1.0×10^4 MPa, and Poisson's ratio of 0.40.

Rock strength parameters varied as well. Internal cohesion was determined from results of uniaxial compressive strength tests (Petrov, 2006). In this case, the Coulomb's limit condition can be written as follows (Rebetsky, 2007):

$$\begin{aligned}\tau_c &\geq \tau_n - k_c\sigma_n \\ &= \sigma\left[0.5\sin 2\alpha_c - k_c(4/3 - \cos 2\alpha_c)\right],\end{aligned} \quad (7)$$

where $\sigma > 0$ is the axial compressive stress (positive compression), k_c is the coefficient of internal friction for brittle failure ($\cot 2\alpha_c = k_c$), τ_c is the internal cohesions for brittle failure.

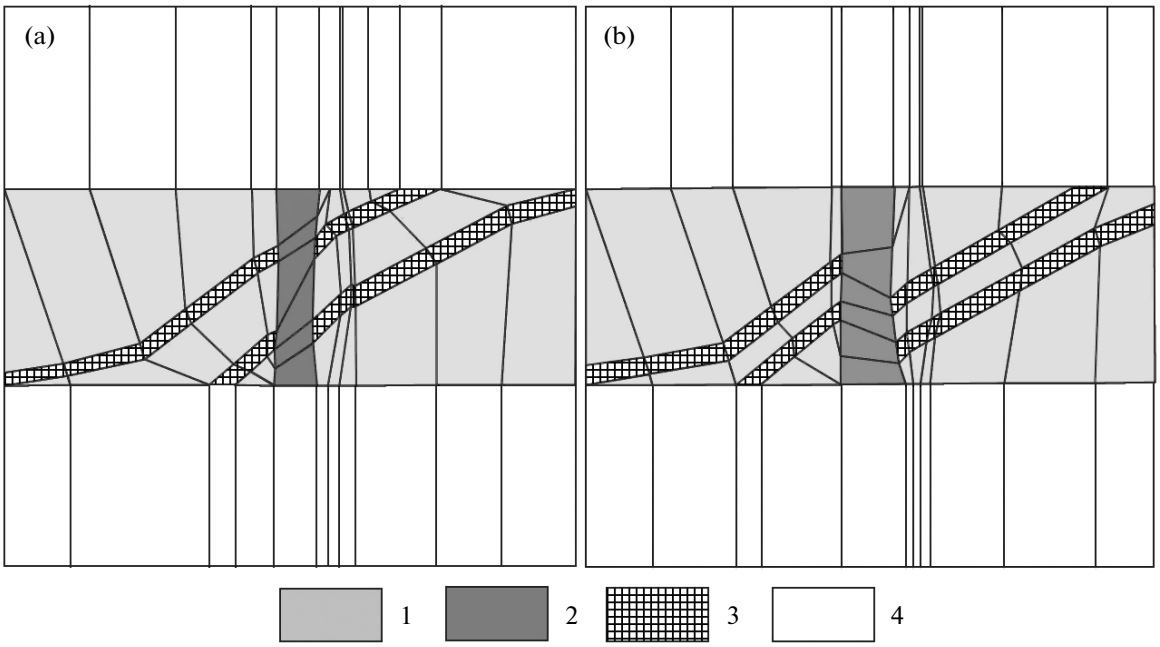

Fig. 9. Main and additional elements in the upper (a) and lower (b) surfaces of the tectonophysical model. (1) Central part (core) of the model, (2) fault, (3) K-feldspathized rocks and albitites, (4) additional blocks needed to extend the model for 350 m along strike, on both sides of the central part of the fault zone. Vertical surfaces are oriented at 30°.

By varying values of the coefficient of friction from 0.5 to 0.7 (according to the experimental results of Byerlee, 1978; Brace, 1978; Stavrogin and Protosenya, 1992 and others, k_c for a wide range of rock types varies from 0.4 to 0.8) and taking experimental results (Table 1) as a basis of defining the ultimate uniaxial compressive load (σ) required to cause brittle failure of the rocks, we can estimate the value of internal cohesion τ_c.

From the relation (7) for $k_c = 0.5,\ 0.6,\ 0.7$, we can determine:

$$\tau_c \geq (0.29,\ 0.37,\ 0.45)\,\sigma \qquad (8)$$

In our further calculations, we will use the value of internal cohesion corresponding to $\tau_c = 0.4\sigma$. Considering this and the data for the uniaxial compressive strength, the experimental results are shown in Table 2.

The model medium for all layers (the main layer and three additional layers) used in numerical experiments was taken to be an elastoplastic body. The plastic limit for the three lower layers (the main layer and the first two additional layers) was determined in the same way as for the Drucker–Prager body (Drucker and Prager, 1952):

$$Y_c \geq I_2 - \varphi p^*, \qquad (9)$$

and for the uppermost (additional layer 3) layer it was determined as for the Mises body:

$$Y_c \geq I_2, \qquad (10)$$

where Y_c is the plastic limit, φ is the plastic friction coefficient, I_2 is the second invariant of deviatoric stress, which is defined by maximum shear stress values (τ) and the kind of the stress state given by the Lode–Nadai coefficient (μ_σ) (Rebetsky, 2007), and p^* is the effective pressure defined as the difference between the tectonic stress in solid rocks (p) and the pressure of the fluid in the pore space (p_{fl}):

$$I_2 = \tau(3 - \mu_\sigma^2)/3, \quad p^* = p - p_{fl}. \qquad (11)$$

In our calculations, the plasticity parameters Y_c and φ are set to the brittle strength parameters τ_c and k_c assuming (Nikolaevskii, 1996) that cataclastic flow in the upper crust may occur due to micro- and macrofracturing while true plastic deformation can be achieved only at lower crustal levels. Therefore, the parameters used in this study should be considered effective.

Since the tectonic pressure p is largely (up to 95%) a function of the lithostatic pressure (p_{lt}) and the distribution of the fluid pressure in the upper crust (to depths of 2–3 km) can be regarded as close to hydrostatic pressure ($p_{hy} = 0.38p_{lt}$), the weight of a column of liquid at a given depth, then the equation (9) can be rewritten as follows:

$$\begin{aligned} Y_c &\geq I_2 - \varphi(p_{lt} - p_{fl}) \\ &= I_2 - 0.62\varphi p_{lt} = I_2 - 0.62\varphi p. \end{aligned} \qquad (12)$$

Assuming $\varphi = k_c = 0.64$, we obtain

Table 2. Brittle strength parameters of rocks derived from experiments (Table 1) and internal friction coefficient $k_c = 0.64$ ($\tau_c = 0.4\sigma$)

Rock type	Internal cohesion (MPa)
Late Paleozoic host granites	84
Late Paleozoic K-feldspathic rocks and albities	94
Late Mesozoic hydromicatized rocks	74

$$Y_c \geq I_2 - \varphi(p_{lt} - p_{fl}) = I_2 - 0.62\varphi p_{lt} = I_2 - 0.4p. \quad (13)$$

The equality in (10) and (13) marks the transition from pure elastic to elastoplastic deformation in the finite element.

Since the calculations account for a higher degree of rock fracturing in the fault zone of the main layer and additional layers, the plastic friction coefficient was reduced by 50%. These layers were given lower values of plastic limit and higher values of Poisson's ratio (up to 0.35–0.4) (Table 3). In this case, the influence of the first upper layers on the stress state in the lower ones can be determined to be similar to a uniformly distributed load equal to the weight of these layers.

Boundary conditions and internal force model. The earlier reconstruction of the tectonic stress field shows that the fault framework at the Antei deposit was formed during four stages. These data allowed us to formulate boundary conditions imposed by the adjacent geological bodies during the late Mesozoic mineralization stage. Our models were design to study the stress state associated with the body (gravity) forces, i.e., the gravitational stress state.

In natural objects, the stress state is caused by many factors. Understanding the mechanisms for the generation of stresses in natural objects using numerical models requires a stepwise approach, which would allow the explanation of each action. With this approach, the selection of the loading and boundary conditions for the created geometric and rheological models was preceded by the analysis of possible forces acting on the rock massif within the Antei deposit.

The first load is interpreted to be associated with the own weight of the rocks forming the gravitational stress state. In this connection, of particular importance are the data on the depth of erosion and absolute paleostress magnitudes. In the case of the Antei deposit located within the area of the collapse caldera confined to a zone of rifting, the depth to the erosional surface can be neglected. On this basis, we can determine that the difference, if any, between the absolute magnitudes of normal principal paleostresses and those of the actual stresses at the Antei deposit was minor. The actual stress magnitude at a depth of 750 m (level 12) considering the weight of overburden averaged 18.82 MPa and 5.62 MPa (at specific weight of 2.51 g/cm^3) for vertical and horizontal stresses, respectively (Kozyrev et al., 2014).

Further studies are needed to estimate the depth of formation of this deposit using two approaches. The first approach proposed by André et al. (2001) is based on the analysis of the spatial distribution of the quartz veins and empirical failure criteria for quartz-containing rocks, coupled with pressure values quantified from fluid inclusion studies of quartz. Using this approach provided absolute magnitudes of the three normal stresses under hydrostatic conditions during the formation of quartz veins in the Soultz-sous-Forets granites of the Rhine graben. A comparison of the estimated paleostress magnitudes and the actual stress measured during hydrofracturing tests in the GPK 1 well indicated a difference of 5–10 MPa at a depth of 1400 m. This depth interval was characterized by slightly lower actual stress magnitudes compared to those of the paleostresses while in the shallower zone these values were very close to each other. The second approach uses data on pressure variations in fluid inclusions from maximum to minimum values, taking into account the restrictions to the physical limits of this range based on lithostatic and hydrostatic fluid pressure (Prokof'ev, Pek, 2015). The combination of these data with the spatial distribution of veins and strength parameters of rock will enable a more precise determination of the absolute paleostress magnitudes during different stages of hydrothermal ore formation at the Antei deposit.

As shown above, the tectonic framework of the deposit area was the result of strike-slip movement along the submeridional fault zone. Therefore, the external stress regime manifested in horizontal shearing represents an additional load, which produces additional stresses relative to the purely gravitational stress state. However, our tectonophysical models were prescribed zero displacement at their boundaries, based on the considerations discussed below.

One of the currently debated issues of tectonophysics and geodynamics is the role of latent stresses (Ponomarev, 2008) and the role of the gravitational stress state as a key factor producing residual compressive stresses acting in the horizontal direction during uplift and erosion (Rebetsky, 2008a). It should be noted that stresses refer those components of the stress tensor responsible for macro- and megascopic brittle

Table 3. Mechanical and strength properties of discrete model layers used in numerical simulation

Rock type	Density, g/cm^3	Young's modulus (GPa)	Poisson's ratio	Ductility ratio	Plasticity limit (MPa)
Main layer and additional layer 1					
Late Paleozoic host granites	2.51	64	0.23	0.4	84
Late Paleozoic K-feldspathic rocks and albities	2.56	76	0.21	0.4	94
Late Mesozoic hydromicatized rocks	2.46	60	0.25	0.2	74
Additional layer 2					
Late Mesozoic trachydacites	2.40	40	0.35	0.2	20
Additional layer 3					
Late Mesozoic felsites	2.40	10	0.405	0.0	10

failure of rock grains and crystals, i.e., deviatoric stresses.

The gravitational state of stress in a rock mass is developed simultaneously with the formation of a rock massif. It is thought (Heim, 1988) that body forces are capable of creating the stress that is equal in all direction to lithostatic pressure $p_{lt} = \rho g h$ (h is the burial depth of the rock, ρg is the average specific density of the overlying rock). It was shown previously (Rebetsky, 2008b) that such a stress state is developed under conditions of elastoplastic gravitational compaction, when the residual horizontal strain induced by the rock under its own weight in the conditions of lateral constraint cause an increase of horizontal compressive stresses. In this case, vertical compressive stresses would be equal to or slightly higher than the horizontal compressive stresses.

In the upper crust where the lithostatic and fluid pressures are not high enough (and the distribution of the fluid pressure at depth obeys the hydrostatic law), the vertical and horizontal compressive stresses may not be fully equalized, since the rock retains its strength to resist relatively high deviatoric stresses. This predetermines the presumably large effect of body forces on the development of deviatoric stresses in rock masses at the Antei deposit.

It is known that during burial rocks (e.g., in sedimentary basins) are subjected to increasing vertical lithostatic pressure and fluid pressures may rise to exceed hydrostatic values (the weight of water column) and approach locally to lithostatic values. This causes an increase in additional compressive stresses due to gravitational compaction. However, the vertical stresses still remain greater than the horizontal ones.

In the areas of uplift and erosion, the slow relaxation of horizontal compressive stresses accumulated at deep crustal levels (Nikolaevskii, 1996) is caused by the absence of effective relaxation mechanisms (dislocation plasticity is active only near and below the Moho). These stresses should be regarded as residual gravitational stresses (Rebetsky, 2008c), serving as the third factor in the studied forces associated with the formation of the rock massif within the Antei deposit.

Latent stresses (Ponomarev, 2008) appear to be associated with macroscopic heterogeneity of rocks, which produces mutually balanced residual stresses at the aggregate and grain scale during quasi-plastic deformation. At present, this kind of the stress state cannot be estimated using mechanical equations. However, accounting for latent stresses induced by elastoplastic deformation through the decrease in the effective strength of rocks will be the focus of our further study.

The paleotectonic reconstruction of ore formation should also consider depth-related changes in the general tectonic situation within granitic massifs. For example, a comparison of the horizontal and vertical magnitudes derived from in situ measurements during hydraulic fracturing conducted at the Aspo hard rock laboratory, Sweden, (Ask, 2003) revealed several horizons with different tectonic regimes (from top downward): a compressive tectonic regime (reverse faulting) develops from the ground surface to a depth of 230 m, where it gives way to shearing (strike-slip faulting) at 230–500 m, which again becomes compression below a depth of 500 m down to the level of 750 m. Our calculations of stresses in rock masses at the Antei deposit indicate the possibility for the transition from shearing to normal faulting regime at level 14 (at a depth of 870 m from the surface). The reconstruction of the dynamics of the tectonic stress field during ore formation requires further investigation.

Gravitational stress state of the rock massif. The proposed 3D model was initially calculated for a purely elastic state. For this purpose, strength parameters in input files that define the properties for the main and the first additional rock layer were set an order of magnitude higher (than those presented in the last column of Table 3) to ensure that the plastic limit is not reached. For this case the maximum shear stress can

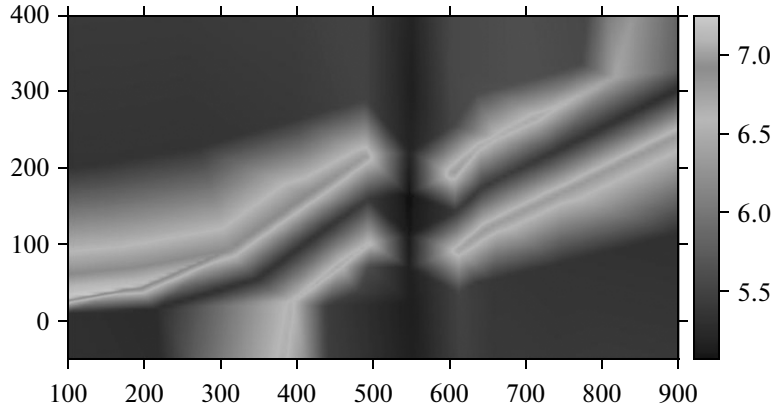

Fig. 10. Distribution of maximum shear stresses (MPa) in the main layer at a depth of 660 m for a purely elastic state.

be assumed to be $\tau = \nu / (1 - \nu)\rho g h$,, where ν is the Poisson's ratio.

Numerical modeling of the main layer at a depth of 660 m shows that the maximum stress is associated with vein-like bodies of K-feldspar rocks and albitites. The most illustrative data were collected for maximum shear stresses (Fig. 10), confining pressure and values of the Lode–Nadai coefficient defining the shape of the stress ellipsoid (Rebetsky, 2007).

For host granites, the stress ellipsoid corresponds to uniaxial compression and represents triaxial stress for vein-like bodies of K-feldspar rocks and albitites. Note that at this depth and given similar mechanical properties of the rock (homogeneous model) the maximum shear stresses should be equal to 5.5 MPa at the purely elastic stage of deformation. Under such deformation conditions the maximum shear stresses cannot exceed one-third of the lithostatic pressure. Such values of maximum shear stress were recorded in the host granites, while they are lower by 0.3–0.6 MPa in hydromicatized rocks of the fault zone and higher by 1.0–1.6 MPa in K-feldspathized and albitized rocks.

The high values of deviatoric stresses that also define the high values of maximum shear stresses in vein-like bodies of K-feldspar rocks and albitites are associated with a spatial heterogeneity of elastic properties. These rocks are characterized by higher values of the Young's modulus (by almost 20%) compared to host granites (Table 3). Therefore, the K-feldspathized and albitized veins should be regarded as a rigid framework of the studied geological medium. During deformation induced by the action of body forces, K-feldspathized and albitized rocks are less susceptible to deformation in the vertical direction than host granites due to their greater rigidity. As a result, some portions of gravity load are transferred from granites to K-feldspar and albitized veins and cause elevated levels of deviatoric stresses, which would be much higher than those imposed on a purely elastic massif with homogeneous rock properties.

Strength data (Table 3) indicate that the rocks in the main layer are in the purely elastic state of stress while plastic deformation is observed only locally in the above layers. However, structural and tectonophysical observations in underground mine workings reveal that the rocks of the fault zone underwent irreversible cataclastic (quasi-plastic) deformation due to shear displacement along macro- and microscopic fractures. It is obvious that plastic deformation can be calculated by reducing the plasticity limit for the model material. Such a reduction underlies the well-known fact that rock strength measured from laboratory tests on small-scale rock samples is many times (or even an order of magnitude) larger than the effective strength of the larger rock massif. This is caused by numerous natural defects always present in a rock massif as well as by the fact that the strength of the large objects is dependent on the strength of its weakest structural element. In this connection, strength values used for further calculations are lower by two orders of magnitude than those presented in Table 3.

Numerical modeling of the stress state of the main layer at a depth 660 m for the purely elastic model (strength parameters for the main layer and additional layer 1 were reduced by two orders of magnitude) shows that the highest values of the maximum shear stresses (about 6 MPa) are associated with vein-like bodies of K-feldspathized and albitized rocks. The stress ranges are estimated to be 2.7–4.0 MPa for the hydromicatized fault zone and 4.6–5.0 MPa for the host granites. In the fault zone, the highest stresses are associated with the intersections of K-feldspathized and albitized veins with the fault. In case of the elastoplastic state, the maximum shear stresses decrease by 1 MPa in host granites, 0.6 MPa in K-feldspathized and albitized veins, and 2.3 MPa in hydromicatized rocks of the near-fault zone compared to those determined for the purely elastic state. The tectonic stress magnitude exceeds the values used in the purely elastic model by 1.5–2.0 MPa for host granites and by 0.5–1.0 MPa for feldspathized and albitized veins. The dif-

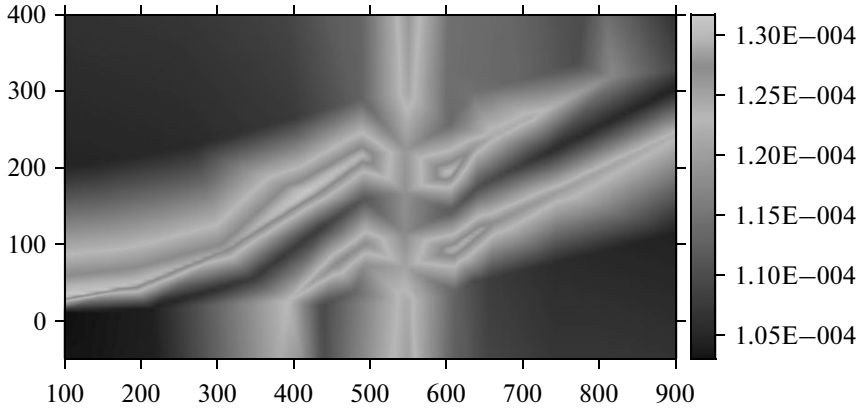

Fig. 11. Distribution of maximum shear in the main layer at a depth of 660 m for an elastoplastic state.

ferences are also noted for the distribution of the Lode–Nadai coefficient, particularly in the fault zone. The evolution of plastic deformations can be estimated from the maximum shear strain presented in Fig. 11.

It is interesting to note that large-scale plastic deformations were reported from K-feldspar and albitized veins and from the hydromicatized fault zone as well. The maximum values of this parameter are measured at the intersection between the fault zone and veins.

The analysis confirms the increment of maximum shear stresses in model layers with depth. The magnitudes of these stresses in the K-feldspathized and albitized veins of additional layer 1 approach those of the granites of the main layer. The stress magnitudes in the hydromicatized fault zone also change with depth.

Note that the results of the analysis of rock deformation reflected in the model gravity stress state show good agreement with the results of acoustic emission monitoring performed at the Institute of Mining, Far East Branch of the Russian Academy of Sciences (Rasskazov et al., 2012). The results show that in existing mining and geological conditions the areas of high acoustic emission levels are spatially associated with vein-like bodies of K-feldspar rocks and albitites.

In our further study we will analyze the influence of residual stresses on the overall stress state of the rock massif within the Antei deposit and calculate the effects of shearing along the strike of the ore-controlling fault zone on the stress state of rocks with implications for the sequence of geodynamic events. The calculations will be based on the analysis of a relationship between magnitudes of shear forces and deviatoric stresses.

CONCLUSIONS

1. We present methodological approaches to the study of the tectonophysical conditions of the formation of hydrothermal ore deposits, using a combination of modern structural, geological, petrophysical and tectonophysical techniques, including the quantitative assessment of the stress–strain conditions. The Antei Mo–U deposit of Transbaikalia was chosen as a unique object for reconstruction of paleotectonic and fluid flow conditions during formation of hydrothermal mineralization. The structural and geological studies show that the fault framework of the deposit was formed in four tectonic stages, three of which took place in the geologic past and one of which reflects recent geologic history. Each tectonic stage was characterized by different parameters of the tectonic stress–strain field, fault kinematics, and conditions of mineral formation.

2. The results of structural and petrophysical studies were used to establish variations in petrophysical properties (density, effective porosity, wet- and dry-rock S- and P-wave velocities, dynamic Young's modulus, shear modulus, and bulk modulus, Poisson's ratio) of rocks and the relationship between density and elastic parameters of granitoids, on the one hand, and the type and intensity of low-and high-temperature preore, synore, and postore hydrothermal–metasomatic alteration, and the intensity of faulting, on the other hand. These results, coupled with the data on structural geology, mineralogy and petrography of the rocks, allowed the assigning of boundary conditions for a 3D tectonophysical model of the rock massif at the Late Meosozoic stage of mineralization.

3. The reconstruction of the dynamics of the tectonic stress field in the rock massif was performed on the basis of the numerical model of gravitational body forces. The mechanisms responsible for the generation of tectonic stresses and stress regime at the Antei deposit were modeled with the finite-element method. For the calculations we used geometric, rheological, and internal force models to describe three main elements of the deposit such as Late Paleozoic host granites, vein-like bodies of Late Paleozoic K-feldspathic and albititic metasomatic rocks, and a fault zone surrounded by Late Mesozoic hydromicatized rocks and

ore bodies inside the faults. The 3D model comprises four layers, with the main layer being the lowest one, corresponding to the geologic section between levels 9 and 12 located at depths of 568 and 750 m, respectively. The upper three layers are used to extend the model to the day surface; they reflect the action of gravitational body forces and progressive diminishing (when approaching to the surface) of the reduction of the rigidity and strength of rocks.

4.The calculation of the effect of the 3D stress state on gravitational forces was performed for the purely elastic and postcritical elastoplastic stages of deformation. The results show that the domains of most intense brittle deformation are confined to vein-like bodies of elastic K-feldspar rocks and albitites, which acted as concentrators of edge-induced stresses within the host granites. The action of oriented stress at the intersections of K-feldspathized and albitized zones with fluid-conducting faults created favorable conditions for the circulation of mineralizing fluids and the formation of ore shoots. This factor should be taken into account in forecasting ore mineralization at deep levels of the deposit.

ACKNOWLEDGMENTS

The authors are deeply indebted to A.A. Pek (Institute of Geology of Ore Deposits, Petrography, Mineralogy and Geochemistry, Russian Academy of Sciences) and P.A. Ignatov (Russian State Geological Prospecting University) for helpful discussions on the manuscript. We also thank our colleagues R.M. Nasimov (Institute of Physics of the Earth, Russian Academy of Sciences), O.V. Andreeva (Institute of Geology of Ore Deposits, Petrography, Mineralogy and Geochemistry, Russian Academy of Sciences), J. Hammer (Federal Institute for Geosciences and Natural Resources, Hannover, Germany), M. Lespinasse (University of Lorrain, Nancy, France), and S.I. Shchukin (Priargunsky Industrial Mining and Chemical Corporation, Krasnokamensk) for long-term effective cooperation and their assistance with the solution of many problems discussed in the study.

This study was supported by the Division of Earth Sciences, Russian Academy of Sciences (program no. 2) and the Russian Foundation for Basic Research (project no. 15-05-01369_a).

REFERENCES

Aleshin, A.P., Velichkin, V.I., and Krylova, T.L., Genesis and formation conditions of deposits in the unique Strel'tsovka Molybdenum–Uranium ore field: New mineralogical, geochemical, and physicochemical evidence, *Geol. Ore Deposits*, 2007, vol. 49, no. 5, pp. 392–412.

André, A.-S., Sausse, J., and Lespinasse, M., New approach for the quantification of paleostress magnitudes: application to the Soultz vein system (Rhine graben, France), *Tectonophysics*, 2001, no. 336, pp. 215–231.

Andreeva, O.V., Aleshin, A.P., and Golovin, V.A., Vertical zonality of wall rock alterations at the Antei–Streltsovsk uranium deposit, eastern Transbaykal region, *Geol. Ore Deposits*, 1996, vol. 38, no. 5, pp. 353–366.

Andreeva, O.V. and Golovin, V.A., Metasomatic processes in uranium ore deposits of Tulukuev caldera in the East Transbaikal region (Russia), *Geol. Ore Deposits*, 1998, vol. 40, no. 3, pp. 184–198.

Angelier, J., Tectonic analysis of fault slip data sets, *J. Geophys. Res.*, 1984, vol. 89, no. B7, pp. 5835–5848.

Ask, D., Evaluation of measurement-related uncertainties in the analysis of overcoring rock stress data from Äspö HRL, Sweden: A case study, *J. Rock Mech. Min. Sci*, 2003, no. 40, pp. 1173–1187.

Atlas strukturno–morfologicheskikh tipov rudnykh obrazovanii Strel'tsovskogo rudnogo polya (Atlas of Structural–Morphological Types of Ore Structures of the Sretl'tsovskoe Ore Field), Irkutsk: Fondy Sosnovskogo PGO, 1982.

Boullier, A.-M., Ohotani, T., Fujimoto, K., Ito, H., and Dubois, M., Fluid inclusions in pseudotachylytes from the Nojima fault, Japan, *J. Geophys. Res.*, 2001, vol. 106, no. B10, pp. 21965–21977.

Brace, W.F., Volume changes during fracture and frictional sliding: A review, *Pure Appl. Geophys.*, 1978, vol. 116, p. 603–614.

Burmistrov, A.A., Starostin, V.I., Dergachev, A.L., and Petrov, V.A., *Strukturno-petrofizicheskii analiz mestorozhdenii poleznykh iskopaemykh* (Structural and Petrophysical Analysis of Mineral Deposits) 2nd revised edition, Moscow: MAKS, 2009.

Byerlee, J.D., Friction of rocks, *Pure Appl. Geophys.*, 1978, vol. 116, pp. 615–626.

Chernyshev, I.V. and Golubev, V.N., The Streltsovskoe deposit, Eastern Transbaikalia – Isotope dating of Mineralization in Russia Largest Uranium Deposit, *Geochem. Int.*, 1996, vol. 34, no. 10, pp. 834–846.

Cowie, P.A., A healing-reloading feedback control on the growth rate of seismic faults, *J. Struct. Geol.*, 1998, vol. 20, no. 8, pp. 1075–1087.

Cox, S.F., Coupling between deformation, fluid pressures, and fluid flow in ore-producing hydrothermal systems at depth in the crust, *J. Econ. Geol. 100th Ann. Vol.*, 2005, p. 39–75.

Di Toro, G., Pennacchioni, G., and Teza, G., Can pseudotachylytes be used to infer earthquake source parameters? An example of limitations in the study of exhumed faults, *Tectonophysics*, 2005, no. 402, pp. 3–20.

Drucker, D.C. and Prager, W., Soil mechanics and plastic analysis of limit design, *Q. Appl. Math.*, 1952, vol. 10, no. 2, p. 157.

Dykhuizen, R.C., Diffusive matrix fracture coupling including the effects of flow channeling, *Water Resour. Res.*, 1992, no. 28, pp. 2447–2450.

Etchecopar, A. and Mattauer, M., Methodes dinamique d'analyse des populations de failles, *Geol. Soc. Am. Bull.*, 1988, no. 8, pp. 289–302.

Geologicheskoe stroenie Chitinskoi oblasti. Ob"yasnitel'naya zapiska k geologicheskoi karte masshtaba 1 : 500000 (Geological Structure of the Chita District. Explanatory Notes for the Geological Map, 1 : 500000 scale), Rutshtein, I.G. and Chaban, N.N., Eds., Chita: GGUP Chitageols'emka, 1997, p. 239.

Golubev, V.N., Age of dispersed uranium mineralization in rocks of the framework of the Strel'tsovka uranium ore field and the Yamsky site, Eastern Transbaikal region, *Geol. Ore Deposits,* 2011, vol. 53, no. 5, pp 401–411.

Gushchenko, O.I., Kinematic analysis of fracture structures during reconstruction of tectonic stress fields, in *Polya napryazhenii i deformatsii v litosfere* (Stress and Strain Fields of the Lithosphere), Moscow: Nauka, 1979, pp. 7–25.

Gzovskii, M.V., *Osnovy tektonofiziki* (Fundamentals of Tectonophysics) Moscow: Nauka, 1975.

Heim, A., *Mechanismus der Gebirgsbidung. Bale*, 1988.

Hudson, J.A., Cornet, F.H., and Christiansson, R., ISRM suggested methods for rock stress estimation-Part 1: Strategy for rock stress estimation, *J. Rock Mech. Min. Sci.*, 2003, no. 40, pp. 991–998.

Ishchukova, L.P., Modnikov, I.S., Sychev, I.V., et al., Uranovye mestorozhdeniya Strel'tsovskogo rudnogo polya v *Zabaikal'e* (Uranium Deposits of the Strel'tsovskoe Ore Field in Transbaikalia), Irkutsk: Tip. "Glazovskaya", 2007.

Kozyrev, A.A., Semenova, I.E., and Avetisyan, I.M., Creation of a discrete geochemical model for the Antei deposit as a basis for predicting strain–stress state of a rock massif, *Gornyi Inf. Anal. Byull.*, 2014, no. 4, pp. 33–40.

Laverov, N.P., Petrov, V.A., Poluektov, V.V., Nasimov, R.M., Hammer, J., Burmistrov, A.A., and Shchukin, S.I., The Antei uranium deposit: a natural analogue of an SNF repository and an underground geodynamic laboratory in granite, *Geol. Ore Deposits*, 2008, vol. 50, no. 5, pp. 339–361.

Lin, A., Tanaka, N., Uda, S., and Satish-Kumara, M., Repeated coseismic infiltration of meteoric and seawater into deep fault zones: a case study of the Nojima fault zone, Japan, *Chem. Geol.*, 2003, vol. 202, pp. 139–153.

Lukin, L.I., Chernyshev, V.F., and Kushnarev, I.P., *Mikrostrukturnyi analiz* (Microstructural Analysis), Moscow: Nauka, 1965.

Mal'kovskii, V.I. and Pek, A.A., *Vliyanie razryvnykh narushenii na protsessy flyuidnogo teplomassoperenosa v zemnoi kore* (The Effect of Faults on Fluid Heat and Mass Transfer in the Earth's Crust), Moscow: IFZ RAN, 2014.

Marrett, R. and Peacock, D.C.P., Strain and Stress, *J. Struct. Geol.*, 1999, no. 21, pp. 1057–1063.

Melosh, H., Impact Cratering: A Geological Process, New York: Oxford University Press, 1989.

Mironenko, M.V., A physicochemical model of hydrothermal mineral formation at the Antei deposit, in *Materialy po geologii uranovykh mestorozhdenii* (Trans. Geology of Uranium Deposits), issue 93, Moscow: VIMS, 1985, pp. 83–87.

Naumov, G.B., Mironenko, M.V., Salazkin, A.N., et al., New data on geochemical conditions of the formation of ore deposits at the Strel'tsovskoe ore field and their practical significance, in *Materialy po geologii uranovykh mestorozhdenii* (Trans. Geology of Uranium Deposits), issue 93, Moscow: VIMS, 1985, pp. 65–82.

Nguyen, P.T., Cox, S.F., Harris, L.B., and Powell, C., MCA., Fault-valve behaviour in optimally oriented shear zones: an example at the Revenge gold mine, Kambalda, Western Australia, *J. Struct. Geol.*, 1998, vol. 20, no. 12, pp. 1625–1640.

Nikolaev, P.N., *Metodika tektonodinamicheskogo analiza* (Methods of Tectonodynamic Analysis), Moscow: Nedra, 1992.

Nikolaevskii, V.N., *Geomekhanika i flyuidodinamika* (Geomechanics and Fluid Dynamics), Moscow: Nedra, 1996.

Nordqvist, A.W., Tsang, Y.W., Tsang, C.-F., et al., Effects of high variance of fracture transmissivity on transport and sorption at different scales in a discrete model for fractured rocks, *J. Contam. Hydrol.*, 1996, no. 22, pp. 39–66.

Oliver, N.H.S., Ord, A., Valenta, R.K., and Upton, P., The role of rock rheological heterogeneity in fluid flow and epigenetic mineralization, with examples from the Mt Isa district, *Rev. Econom. Geol.*, 2001, vol. 14, pp. 51–74.

Petrov, V.A., Tectonodynamic conditions of radioactive waste disposal in crystalline rocks, *Doctoral (Geol. Mineral.) Dissertation*, Moscow: IGEM RAN, 2006.

Petrov, V.A., Tectonophysical conditions of the formation of volcanotectonic structures of the East Tarnsbaikalian uranium province, in *Tezisy nauchnoi konferentsii* (Proceedings of the Scientific Conference), Moscow: IGEM RAN, 2007, pp. 140–144.

Petrov, V.A., Poluektov, V.V., Andreeva, O.V., Golovin, V.A., Shchukin, S.I., Prosekin, B.A., Nasimov, R.M., and Burmistrov, A.A., Fault framework, mineralogical and chemical composition, petrophysical properties and stress–strain state of the rocks at the Antei deposit, in *Tezisy nauchnoi konferentsii* (Proceedings of the Scientific Conference), Moscow: IGEM RAN, 2007, pp. 148–152.

Petrov, V.A., Poluektov, V.V., Nasimov, R.M., Shchukin, S.I., and Hammer, J., Natural and technogenic changes in the mode of rock deformation in the uranium deposit in granites, *Izv. Phys. Solid Earth*, 2009, vol. 45, no. 11, pp. 1012–1018.

Petrov, V.A., Tectonophysical and structural-petrophysical indicators of fluid migration in fault zones and methods of their investigation, in *Sovremennaya tektonofizika. Metody i rezul'taty* (Modern Tectonophysics. Methods and Results), vol. 2, Moscow: IFZ RAN, 2011, pp. 94–108.

Petrov, V.A., Poluektov, V.V, Nasimov, R.M., Burmistrov, A.A, Shchukin, S.I., and Hammer, J., A study of natural and anthropogenic processes in granites of uranium deposits for substantiation of long-term safe SNF disposal, in *Ekstremal'nye prirodnye yavleniya i katastrofy. T. 2 Geologiya urana, geoekologiya, glyatsiologiya* (Extreme Natural Phenomena and Catastrophes. Vol. 2), Moscow: IFZ RAN, 2011, pp. 124–138.

Petrov, V.A., Ustinov, S.A., Poluektov, V.V., and Prokof'ev, V.Yu., Reconstruction of migration paths and conditions for ore-bearing hydrothermal fluids: Structural–geological and thermobarogeochemical approach, *Vestnik RFFI*, 2013, no. 1, pp.27–33.

Petrov, V.A., Andreeva, O.V., and Poluektov, V.V., Effect of petrophysical properties and deformation on vertical zoning of metasomatic rocks in U-bearing volcanic structures: A case of the Strel'tsovka caldera, Transbaikal region, *Geol. Ore Deposits*, 2014, vol. 56, no. 2, pp. 81–100.

Petrov, V.A., Veselovskii, A.V., Kuz'mina, D.A., Plate, A.N., and Gal'berg, T.V., Three-dimensional GIS-modeling of geodynamic objects and processes, Available from VINITI, 2015, Ser.2, no. 1, pp. 15–21.

Ponomarev, V.S., *Energonasyshchennost' geologicheskoi sredy* (Energy Content of a Geologic Medium), Moscow: Nauka, 2008.

Prokof'ev, V.Yu. and Pek, A.A., Problems in estimation of the formation depth of hydrothermal deposits by data on

pressure of mineralizing fluids, *Geol. Ore Deposits*, 2015, vol. 57, no. 1, pp. 1–20.

Rasskazov, I.Yu., Saksin, B.G., Petrov, V.A., and Prosekin, B.A., Geomechanical conditions and peculiarities of dynamic manifestations of overburden pressure at the Antei deposit, *Fiziko-Tekhnicheskie problemy razrabotki poleznykh iskopaemykh*, 2012, no. 3, pp. 3–13.

Rasskazov, I.Yu., Saksin, B.G., Petrov, V.A., Shevchenko, B.F., Usikov, V.I., and Gil'manova, G.Z Present-day stress-strain state in the upper crust of the Amurian lithosphere plate, *Izv., Phys. Solid Earth,* 2014, vol. 50, no. 3, pp. 444–452.

Rastsvetaev, L.M., A paragenetic structural analysis of faults, in *Problemy strukturnoi geologii i fiziki tektonicheskikh protsessov* (Problems of Structural Geology and Physics of Tectonic Processes), Moscow: Nauka, 1987, pp. 173–230.

Rebetsky, Yu.L., Mechanism of generation of tectonic stresses in the zones of high vertical movements and earthquakes, *Fiz. Mezomekh.*, 2008a, vol. 1, no. 11, pp. 66–73.

Rebetsky, Yu.L., Possible mechanism of horizontal compression stress generation in the Earth's crust, *Dokl. Earth Sci.*, 2008b, vol. 423A, no. 9, pp 1448–1451.

Rebetsky, Yu.L., *Tektonicheskie napryazheniya i prochnost' gornykh massivov* (Tectonic Stresses and Strength of Rock Massifs), Moscow: Nauka, 2007.

Rebetsky, Yu.L., Mechanism of generation of residual stresses and high-magnitude horizontal compressive stresses in the earth's crust of intraplate orogens, in *Problemy tektonofiziki. K 40-letiyu sozdaniya M.V. Gzovskim laboratorii tektonofiziki v IFZ RAN* (Problems of Tectonophysics. On the 40th Anniversary since M.V. Gzovskii's Foundation of the Laboratory of Tectonophysics at the Institute of Physics of the Earth), Moscow: IFZ RAN, 2008.

Reinecker, J., Heidbach, O., Tingay, M., et al., The 2005 release of the World Stress Map. http://www.world-stress-map.org.

Seminskii, K.Zh., *Vnutrennyaya struktura kontinental'nykh razlomnykh zon. Tektonofizicheskii aspekt* (Internal Structure of Continental Fault Zones), Novosibirsk: SO RAN, Filial Geo, 2003.

Shchukin, S.I., Petrov, V.A., Poluektov, V.V., and Ustinov, S.A., Geological database for modeling and prediction of deformation in the rock massif at the Antei deposit of the Strel'tsovskoe ore field, *Gorn. Zh.*, 2015, no. 2, pp. 21–26.

Sherman, S.I., Bornyakov, S.A., and Buddo, V.Yu., *Oblasti dinamicheskogo vliyaniya razlomov (rezul'taty modelirovaniya)* (Zones of Fault Dynamic Influence Based on Modeling Results), Novosibirsk: Nauka, 1983.

Shipton, Z.K. and Cowie, P.A., A conceptual model for the origin of fault damage zone structures in high-porosity sandstone, *J. Struct. Geol.*, 2003, no. 25, pp. 333–344.

Sibson, R.H., Implications of fault-valve behavior for rupture nucleation and recurrence, *Tectonophysics*, 1992, vol. 211, pp. 283–293.

Sibson, R.H., Structural permeability of fluid-driven fault-fracture meshes, *J. Struct. Geol.*, 1996, no. 8, pp. 1031–1042.

Sim, L.A., A study of tectonic stresses based on geological indicators (methods, results, recommendations), *Izv. Vyssh. Uchebn. Razved., Geol. Razved.,* 1991, no. 10, pp. 3–27.

Starostin, V.I., Strain–velocity concept of the formation of ore-bearing structures and their typification, *Vestn. Mosk. Univ., Ser. 4: Geol.,* 1994, no. 3, pp. 3–19.

Starostin, V.I., *Strukturno-petrofizicheskii analiz endogennykh rudnykh polei* (Structural–Petrophysical Analysis of Endogenic Ore Fields), Moscow: Nedra, 1979.

Starostin, V.I., *Paleotektonicheskie rezhimy i mekhanizmy formirovaniya struktur rudnykh polei* (Paleotectonic Regimes and Mechanisms of the Formation of Ore Field Structures), Moscow: Nedra, 1988.

Stavrogin, A.N. and Protosenya, A.G., *Mekhanika deformirovaniya i razrusheniya gornykh porod* (Mechanics of Rock Deformation and Failure), Moscow: Nedra, 1992.

Tagami, T., Thermochronological investigation of fault zones, *Tectonophysics*, 2012, vol. 538–540, pp. 67–85.

Vlasov, A.N., Yanovskiy, Yu. G., Mnushkin, M.G., Popov, A.A., Solving geomechanical problems with UWay FEM package, *Computational Methods in Engineering and Science*, Iu, V.P., Ed., Taylor and Francis, 2004, pp. 453–461.

Translated by N. Kravets